Design and Synthesis of Fluorophore-Tagged Disparlure Enantiomers to Study Pheromone Enantiomer Discrimination in the Pheromone-Binding Proteins from the Gypsy Moth, Lymantria Dispar.

Govardhana R. Pinnelli
Simon Fraser University
Erika Plettner (plettner@sfu.ca)
Simon Fraser University https://orcid.org/0000-0001-8934-9791

Research Article

Keywords: Fluorescein, fluorophore-tagged disparlure enantiomers, enantioselective synthesis, cis epoxide, Fluorescence binding assays, click reaction

Posted Date: July 12th, 2021

DOI: https://doi.org/10.21203/rs.3.rs-672921/v1

Design and Synthesis of Fluorophore-tagged Disparlure Enantiomers to Study Pheromone Enantiomer Discrimination in the Pheromone-Binding Proteins from the Gypsy Moth, *Lymantria dispar*.

Govardhana R. Pinnelli, Erika Plettner*

[1]Dept. of Chemistry, Simon Fraser University, 8888 University Dr., Burnaby B. C. V5A 1S6, Canada

* Author for correspondence (plettner@sfu.ca)

Abstract

Fluorescent analogues of the gypsy moth sex pheromone (+)-disparlure (**1**) and its enantiomer (-)-disparlure (*ent*-**1**) were designed, synthesized and characterized. The fluorescently labelled analogues 6-FAM (+)-disparlure **1a** 6-FAM (-)-disparlure *ent*-**1a** were prepared by copper-catalyzed azide-alkyne cycloaddition (CuAAC) of disparlure alkyne and 6-FAM azide. These fluorescent disparlure analogues **1a** *ent*-**1a** were used to measure the disparlure binding to two pheromone-binding proteins from the gypsy moth, *Ldis*PBP1 and *Ldis*PBP2. The fluorescence binding assay using 6-FAM disparlure enantiomers 1**a** and *ent*-**1a** showed that the *Ldis*PBP1 and *Ldis*PBP2 have different binding affinities with **1a** and *ent*-**1a**. The *Ldis*PBP1 has stronger affinity for 6-FAM (-)-disparlure *ent*-**1a**, whereas *Ldis*PBP2 has stronger affinity for 6-FAM (+)-disparlure **1a**, consistent with the findings from previous study with disparlure enantiomers. The 6-FAM disparlure enantiomers appeared to be much stronger ligands for *Ldis*PBPs, with the binding constant (K_d) in nanomolar range, compared to the fluorescent reporter such as 1-NPN (which had K_d values in micromolar range). The fluorescence competitive binding assays were used to determine the displacement constant (K_i) for the disparlure enantiomers in competition with fluorescent disparlure analogues binding to *Ldis*PBP1 and *Ldis*PBP2. The K_i data showed that disparlure enantiomers can effectively displace the fluorescent disparlure from the binding pocket of *Ldis*PBPs.

Keywords Fluorescein, fluorophore-tagged disparlure enantiomers, enantioselective synthesis, cis epoxide, Fluorescence binding assays, click reaction

Introduction

Pheromones are detected by moths using a very organized system, located on the antennae (Krieger and Breer 1999). Pheromones are signals that are transformed into neuronal signals by pheromone sensory neurons found specifically in the antennae of male moths. Antennae of male moths are covered in sensory hairs (sensilla), which are innervated with dendrites of olfactory sensory neurons. Pores in the cuticle of the hairs allow the diffusion of pheromones to the interior, where they first interact with pheromone-binding proteins (PBPs) in the lymph and next with pheromone receptors (PRs). The latter are embedded in the dendritic end of pheromone sensory neurons and are bathed in sensillum lymph (an aqueous solution rich in PBPs, fatty acids and ions). PRs are ion channels that become activated and open upon binding of the pheromone, causing a slow depolarization of the dendritic membrane (Sato et al. 2008; Wicher et al. 2008). The PBPs bind pheromones and other compounds reversibly and selectively, in order to keep them in the lymph.

In the gypsy moth, *Lymantria dispar*, two PBPs have been discovered, *Ldis*PBP1 and *Ldis*PBP2 (Vogt et al. 1989). Both proteins share 50% identity and belong to the insect odorant-binding protein (OBP) family with a long C-terminus. The *Ldis*PBP1 and *Ldis*PBP2 contain 143 and 145 amino acid residues, respectively. Insect PBPs have helical structures, stabilized by three conserved disulfide bridges. Furthermore, PBPs access two structural forms, the A form (usually seen under acidic conditions) (Terrado et al. 2020) and the B form (often found under basic conditions) (Sandler et al. 2000).

Previously, we have shown that (+)-disparlure (**1**), the gypsy moth sex pheromone, and its enantiomer (-)-disparlure (*ent*-**1**) (Fig. 1) bind strongly to *Ldis*PBP1 and *Ldis*PBP2, with opposite enantioselectivity. *Ldis*PBP1 has higher affinity for (-)-disparlure (*ent*-**1**), whereas *Ldis*PBP2 has higher affinity for (+)-disparlure (**1**) (Plettner et al. 2000; Yu and Plettner 2013). This remarkable enantiomer discrimination between (+)-disparlure (**1**) and (–)-disparlure (*ent*-**1**) by the gypsy moth PBPs depends on the non-covalent interactions between these proteins and the pheromone when these molecules collide. Analysis of the sequences of *Ldis*PBPs has revealed the presence of phenylalanine amino acid residues that

are highly conserved among Lepidoptera PBPs: Phe12, Phe36, Phe76, Phe119 (PBP1) and Phe120 (PBP2). These residues interact with the hydrophobic region (hydrocarbon chains) of the ligands when the PBP is in the B form (Sandler et al. 2000; Honson et al. 2003; Sanes and Plettner 2016). Furthermore, the binding site residues that vary between *Ldis*PBPs were found to be: Asn35, Ala73, Leu91, and Ala135 in *Ldis*PBP1, whereas in *Ldis*PBP2 these residues were substituted with Asp35, Thr73, Ile91 and Leu136 (Sanes and Plettner 2016). Our recent NMR and molecular docking studies have demonstrated that the disparlure enantiomers adopt different conformations and orientations in the binding pocket of *Ldis*PBP1 and *Ldis*PBP2 (Pinnelli et al. 2019). In addition, the two PBPs differ in their ligand binding association and dissociation kinetics. Both proteins undergo a two-stage ligand binding process: a rapid association at one or more external site(s), followed by a slow diffusion of the ligand to the interior of the protein. PBP2 binds ligands at its internal binding site very slowly, whereas PBP1 has much faster association and dissociation kinetics (Gong et al. 2009; 2010). We have shown that in PBP2, the enantiomers of disparlure differ in the rate at which they bind to the internal binding site (Gong et al. 2009). However, due to their higher rates, the enantioselectivities of the external binding events in both PBPs and of the internalization of ligands in PBP1 have not yet been studied. To understand the mechanism by which PBPs recognize different ligands, it is necessary to study the kinetics of the association and dissociation processes.

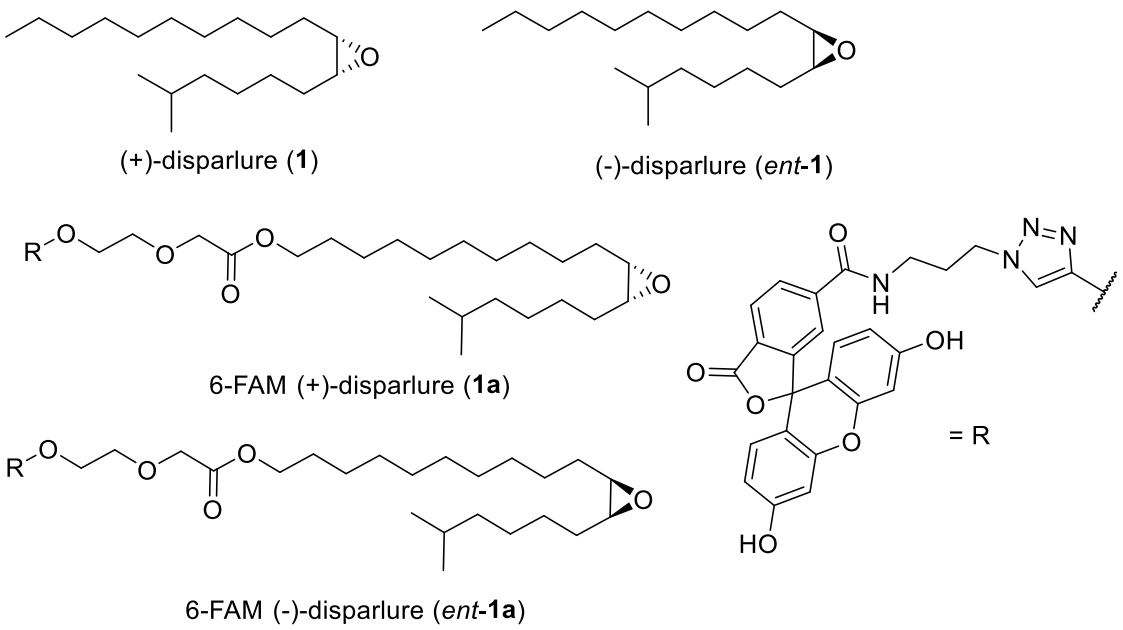

Figure 1. Structures of disparlure enantiomers and their fluorescent analogues.

Ligand-binding experiments between pheromone binding proteins (PBPs) and hydrophobic ligands (*e.g.* pheromones) can be performed in two general ways: 1) the ligand and protein are equilibrated in buffer, and the protein-bound ligand is then separated from the free ligand using filtration (Plettner et al. 2000) or 2) the protein is titrated with a fluorescent reporter such as NPN (N-phenyl-1-napthylamine), and the NPN is then displaced by titration of the PBP-NPN complex with the ligand of interest (Ban et al. 2002, Gong et al. 2010, Gong and Plettner 2011). Disadvantages of equilibrium binding assays are: the adsorption of hydrophobic ligands to vial surfaces and the potential loss of bound ligand during the filtration step, which leads to underestimates of binding affinity. Determination of binding constants of the PBP-ligand complex in the second type of experiment depends on the displacement of the fluorescent reporter by a competing ligand with a concomitant decrease in NPN fluorescence. This type of binding experiment does not require any physical separation of bound ligand from unbound ligand (Ban et al. 2002). However, this approach needs the availability of a fluorescent reporter equipped with good binding strength for the PBP under study, whose fluorescence emission is significantly increased when the reporter binds inside the PBP's binding pocket.

The disadvantage of the use of fluorescent reporters in ligand-binding assays is that various compounds differ in their ability to displace the reporter (due to kinetic factors and incomplete equilibration between aliquot additions during these experiments), rather than reporting the binding strength of the ligand of interest to the PBP. Another disadvantage is the strong fluorescent emission of the reporter in the presence of compounds that are capable of forming micelles (*e.g*. fatty acids or amphiphilic pheromones). In this case, the reporter can occupy the hydrophobic core of the micelle, producing a strong fluorescent peak, indistinguishable from that emitted when the reporter is in the binding pocket of the PBP. An example of this problem can be seen in the study by McAffee et al. (2018) when they titrated OBPs 16 and 18 from the honey bee with oleic acid. Given these drawbacks, kinetic studies with NPN as a reporter are difficult to interpret meaningfully, so we propose that linking the ligand of interest with the fluorescent reporter would solve some of these problems and provide a tool for mechanistic studies between PBPs and their cognate pheromones.

We have covalently linked 6-carboxyfluorescein (6-FAM) to the gypsy moth sex pheromone (+)-disparlure (**1**) and to its enantiomer (-)-disparlure (*ent*-**1**) (Fig. 1) by adding a linker with a terminal alkyne moiety to disparlure and performing a click reaction of the alkyne and 6-carboxyfluorescein azide (6-FAM azide). We choose 6-carboxyfluorescein (6-FAM) as a fluorescent reporter because of its high fluorescence quantum yield (0.93), good water solubility and its derivatives, such as 6-FAM azide, are commercially available. In addition to the high quantum yield, it has excellent absorption and emission properties (Sjöback et al. 1995; Zhang et al. 2014). This is the first report describing the synthesis of a fluorophore-tagged insect pheromone. We expect that these fluorophore-tagged pheromones will provide researchers with a viable alternative to the radiolabeled pheromones and fluorescent probes such as 1-NPN that are used in PBP-pheromone binding assays. To date, the use of fluorophore tagged pheromones as a fluorescent reporter in the study of pheromone binding protein interactions has not been reported.

In this paper, we report the synthesis (Scheme 1) and spectroscopic characterization of fluorophore-tagged disparlure enantiomers 6FAM (+)-disparlure (**1a**) and 6FAM (-)-disparlure (*ent*-**1a**) (Fig. 1), and their binding affinities to two pheromone binding proteins

*Ldis*PBP1 and *Ldis*PBP2 of gypsy moth. The disparlure binding to *Ldis*PBPs was determined by changes in fluorescence emission intensity of the solution containing *Ldis*PBPs and 6-FAM disparlure. The relative changes in fluorescence intensity reflecting binding to *Ldis*PBP1 or *Ldis*PBP2 are quantitated as a function of increasing 6FAM (+)-disparlure (**1a**) or 6-FAM (-)-disparlure (*ent*-**1a**) concentration.

Materials and Methods

General Experimental

All reactions were carried out in the presence of a nitrogen atmosphere and at room temperature unless the reactions were performed in aqueous media or unless otherwise specified. Reactions carried out at -78 °C used a bath of dry ice in acetone. Reactions undertaken at 0 °C utilized a bath of water and ice. Hexanes and ethyl acetate were distilled prior to use. Chemicals and Reagents were used without further purification. Syringes and cannulas were used to transfer reagents. Reactions were monitored by thin layer chromatography (TLC) on aluminum baked silica plates (Merck Silica Gel 60 F254) and products were visualized under UV or stained with phosphomolybdic acid (PMA) or anisaldehyde or potassium permanganate followed by exposure of the stained plates to heat. Silica flash chromatography (Fisher Silica Gel 60 40-63 μm) was undertaken to purify crude reaction mixtures using hexanes/ethyl acetate mixture. The enantiomeric excess (*ee*) was analyzed on an Agilent 1260 HPLC equipped with a chiral column (Phenomenex, Lux 5u cellulose-2, 250×4.60 mm Lux 5μm Cellulose-2) and variable wavelength detector (VWD). The HPLC chromatograph was programmed with hexanes/isopropanol/DEA (90:10:0.1). Optical rotations were recorded on a Perkin-Elmer Polarimeter 340 thermostatted to 20 ºC, using the sodium D line.

The ^{1}H NMR spectra were obtained on Bruker DRX 400 and 500 MHz spectrometers in $CDCl_3$. Chemical shifts and coupling constants were reported in parts per million (ppm) and hertz (Hz) respectively. ^{1}H NMR data was reported as follows: chemical shift values (ppm), multiplicity (s = singlet, d = doublet, t = triplet, q = quartet, m = multiplet). ^{13}C NMR spectra were recorded in $CDCl_3$ by using a Bruker DRX 400 MHz or

DRX 500 MHz. ^{13}C NMR data are reported as chemical shift values (ppm). IR spectra were obtained with a Perkin-Elmer Spectrum One FT-IR spectrometer and samples were directly placed on the KBr plates. High-resolution mass spectra (HRMS) were obtained by using positive electrospray ionization (EI) and by the time of flight (TOF) method. The GC-MS analysis was performed using Clarus 690-GC and Clarus SQ8T-MS systems (Perkin Elmer, MA, USA). GC-MS, equipped with a fused silica capillary column (SPB-5, 30 m × 0.25 mm i.d., film thickness 0.25 μm, Supelco, Bellefonte. PA, USA) with positive electron ionization (EI).

PBPs were expressed in *E. coli* with a histidine purification tag, as described before (Terrado et al. 2020). Briefly, they were purified by chromatography on a column of nickel immobilized in iminodiacetic acid agarose resin. The purification tag was removed by digestion with thrombin, and the cleaved protein was isolated by chromatography on a column of carboxymethyl (CM)-functionalized dextran matrix cation exchanger (Sigma Aldrich). The purified protein was delipidated by hydrophobic interaction chromatography on beads of methyl functionalized methacrylate (Bio-Rad, Hercules, CA). Pure, delipidated protein was flash frozen in aliquots and thawed just prior to use in experiments.

General synthetic procedure for preparation of protected alcohols 12, 13 or 20

Three protection groups were tried for the single protection of 1,12-dodecanediol: methoxymethyl (MOM), t-butyldimethylsilyl TBDMS) or benzyl (Bn) (Scheme 2). **Compounds 12 and 13.** To a nitrogen flushed 50 mL flask was added 1, 12-dodecanediol (**11**) (200 mg, 0.990 mmol) *N*,*N*-Diisopropylethylamine (DIPEA, 130 mg, 0.990 mmol) or imidazole (67.4 mg, 0.990 mmol), and dichloromethane (2 mL). Next, either methoxymethyl chloride (MOM-Cl, 80 mg, 0.990 mmol) or t-butyldimethylsilyl chloride (TBDMS-Cl, 150 mg, 0.990 mmol) was added, and the reaction mixture was allowed to stir at room temperature for 4h. The resulting mixture was diluted with dichloromethane (20 mL) and washed with water (10 mL) and saturated NaCl solution (10 mL). The organic phase was dried over Na_2SO_4, filtered and concentrated *in vacuo*. The resulting crude product was purified by silica flash column chromatography (15% EtOAc/hexane) to yield

the product **12** (116 mg, 48%) or **13** (145 mg, 46%). Compound **12**: ^{1}H NMR (400 MHz, $CDCl_3$) δ: 4.60 (s, 2H), 3.61 (t, *J* = 6.6 Hz, 2H), 3.50 (t, *J* = 6.7 Hz, 2H), 3.34 (s, 3H), 1.57 (m, 4H), 1.28 (m, 14H). ^{13}C NMR (125 MHz, $CDCl_3$) δ: 96.49, 68.01, 63.13, 55.19, 32.92, 29.86, 29.70, 29.69, 29.68, 29.67, 29.55, 29.54, 26.32, 25.87. Compound **13**: ^{1}H NMR (400 MHz, $CDCl_3$) δ: 3.66-3.62 (t, *J* = 6.6 Hz, 2H), 3.61-3.57 (t, *J* = 6.6 Hz, 2H), 1.60-1.48 (m, 4H), 1.31-1.25 (m, 14H), 0.89 (s, 9H), 0.05 (s, 6H).

Compound 20: To a cold (0 °C) stirred suspension of NaH (0.534 g, 24.75 mmol) in anhydrous THF (100 mL), 1, 12-dodecanediol (**11**) (5 g, 24.75 mmol) was added. After 30 min stirring at rt, the benzyl bromide (**19**) (4.24 g, 24.75 mmol) was added dropwise, and the reaction mixture was refluxed at 70 °C for 12 h. Then the reaction was quenched with ice-cold water and diluted with EtOAc (100 mL). The aqueous layer was separated and extracted with ethyl acetate (2×50 mL). The organic layers were pooled, washed with brine solution (50 mL), dried over Na_2SO_4, and concentrated under reduced pressure to afford crude product. Purification of the crude product by flash chromatography (silica gel, 80: 20 hexanes: ethyl acetate) yielded 12-(benzyloxy) dodecan-1-ol **20** as a colourless solid (3.2 g, 44%). ^{1}H NMR (500 MHz, $CDCl_3$) δ: 7.37-7.32 (d, *J* = 4.4 Hz, 4H), 7.30-7.26 (m, 1H), 4.52-4.49 (s, 2H), 3.66-3.61 (t, *J* = 6.7 Hz, 2H), 3.48-3.44 (t, *J* = 6.7 Hz, 2H), 1.64-1.54 (m, 4H), 1.50- 1.40 (s, 1H), 1.38-1.26 (m, 16H). ^{13}C NMR (125 MHz, $CDCl_3$) δ 138.64, 128.25, 127.53, 127.37, 72.77, 70.46, 62.99, 32.74, 29.70, 29.52, 29.50, 29.49, 29.48, 29.40, 29.38, 29.35, 26.12, 25.67. IR (neat): 3360, 2922, 2849, 2794, 1116, 1058, 956, 735 cm^{-1}. GCMS (EI) m/z calculated for $C_{19}H_{32}O_2$ $[M]^{+\cdot}$: 292.24; found: 292.30

General procedure for synthesis of MOM or TBDMS protected aldehyde 14, 15 or 21

Compounds **14**, **15** or **21** were prepared by oxidation of the alcohol group of compounds **12**, **13** or **20** with pyridinium chlorochromate (Scheme 2).

The procedure was the same for all three compounds; the one for **21** is given in detail. To a stirred solution of 12-(benzyloxy) dodecan-1-ol (**20**) (2.2 g, 7.48 mmol) in dichloromethane (50 mL), pyridinium chlorochromate (PCC, 1.93 g, 8.97 mmol) was added portionwise at room temperature. After that, the reaction mixture was stirred at room

temperature for 2h. The resulting gummy black residue was diluted with dichloromethane (50 mL) and the supernatant liquid decanted from the gummy black residue. The black residue was washed with dichloromethane (2×50 mL). The combined dichloromethane solution was filtered through a pad of alumina, dried over Na_2SO_4, and concentrated *in vacuo* to yield crude product. Purification of the crude product by flash chromatography (silica gel, 90:10 hexanes: ethyl acetate) yielded 12-(benzyloxy) dodecanal (**21**) as a colourless semi solid (1.94 g, 89%). ^{1}H NMR (500 MHz, $CDCl_3$) δ: 9.76 (s, 1H), 7.35-7.27 (m, 5H), 4.50 (s, 2H), 3.46 (s, 2H), 2.41 (s, 2H), 1.61 (t, *J* = 13.4 Hz, 5H), 1.28 (d, *J* = 13.6 Hz, 18H). ^{13}C NMR (125 MHz, $CDCl_3$) δ: 202.82, 138.63, 128.23, 127.51, 127.35, 72.76, 70.43, 43.83, 29.70, 29.46, 29.41, 29.37, 29.31, 29.25, 29.07, 27.28, 26.10, 22.00. IR (neat): 2925, 2853, 1725, 1101, 735 cm^{-1}. GCMS (EI) m/z calculated for $C_{19}H_{30}O_2$ $[M]^{+\cdot}$: 290.22; found: 290.10

Compound 14: Compound **12** (100 mg, 0.406 mmol), PCC (87 mg, 0.406 mmol), CH_2Cl_2 (2 mL). (Eluent: 7% EA/hexane), 80 mg, 81%.^{1}H NMR (400 MHz, $CDCl_3$) δ: 9.75 (t, *J* = 1.9 Hz, 1H), 4.61 (s, 2H), 3.50 (t, *J* = 6.6 Hz, 2H), 3.35 (s, 3H), 2.40 (td, *J* = 7.4, 1.9 Hz, 2H), 1.59-1.54 (m, 4H), 1.36-1.26 (m, 14H).^{13}C NMR (125 MHz, $CDCl_3$) δ 203.05, 96.51, 68.00, 55.20, 44.04, 29.87, 29.68, 29.63, 29.55, 29.52, 29.47, 29.29, 26.34, 22.21.

Compound 15: The compound **13** (100 mg, 0.316 mmol), PCC (68 mg, 0.406 mmol), CH_2Cl_2 (2 mL). (Eluent: 5% EA/hexane), 80 mg, 92%. ^{1}H NMR (500 MHz, $CDCl_3$) δ: 9.75 (s, 1H), 3.60-3.56 (t, *J* = 6.7 Hz, 2H), 2.43-2.39 (t, *J* = 8.2 Hz, 2H), 1.64-1.58 (p, *J* = 7.3 Hz, 2H), 1.52-1.46 (p, *J* = 6.6 Hz, 2H), 1.30-1.23 (m, 14H), 0.88 (s, 9H), 0.03 (s, 6H). ^{13}C NMR (125 MHz, $CDCl_3$) δ 203.23, 63.46, 44.06, 32.99, 29.72, 29.64, 29.55, 29.54, 29.49, 29.28, 26.11, 26.01, 25.90, 22.18, -5.12.

Preparation of (*R*)-12-(benzyloxy)-2-chlorododecanal (22)

The three aldehydes, **14**, **15** and **21**, were subjected to α-chlorination. The procedure for conversion of **21** to **22** is given. Aldehydes **14** and **15** did not react (Scheme 2). The D-SOMO catalyst **16** (1.10 g, 3.81 mmol) was added to a stirred ice cooled solution of the 12-(benzyloxy) dodecanal (**21**) (2.2 g, 7.65 mmol) in acetonitrile (50 mL) and water (0.3

mL) followed by the addition of $Cu(TFA)_2.H_2O$ (0.430 g, 1.517 mmol), LiCl (0.640 g, 1.517 mmol) and $Na_2S_2O_8$ (2.16 g, 9.103 mmol). The reaction mixture was stirred at 5 °C until dodecanal had been completely consumed (as determined by ^{1}H NMR spectroscopy). After this time, the reaction mixture was treated with water (20 mL) and diluted with ethyl acetate (50 mL), and the phases were separated. The aqueous phase was extracted with ethyl acetate (3×50 mL). The combined organic phases were washed with brine (100 mL), dried over Na_2SO_4, and concentrated *in vacuo* to produce the crude chloroaldehyde. Purification of the crude product by flash chromatography afforded the (*R*)-12-(benzyloxy)-2-chlorododecanal (**22**) as a pale yellow liquid (1.45g, 53.1%). ^{1}H NMR (500 MHz, $CDCl_3$) δ: 9.49 (s, 1H), 7.34 (d, *J* = 4.4 Hz, 5H), 4.51 (s, 3H), 4.19-4.12 (m, 1H), 3.47 (t, *J* = 6.6 Hz, 3H), 1.94 (s, 1H), 1.82 (d, *J* = 37.7 Hz, 1H), 1.62 (d, *J* = 28.2 Hz, 3H), 1.28 (s, 22H). ^{13}C NMR (125 MHz, $CDCl_3$) δ: 195.28, 138.63, 128.24, 127.52, 127.37, 77.15, 72.77, 70.42, 63.92, 31.98, 29.69, 29.41, 29.35, 29.31, 29.18, 28.84, 26.10, 25.45. IR (neat): 2926, 2854, 1725, 1102, 735, 698 cm^{-1}. GCMS (EI) m/z calculated for $C_{19}H_{29}ClO_2$ [M+1]: 325.19; found: 325.30 $[\alpha]^{25}_D$: + 13.4 (c 0.8, $CHCl_3$).

Preparation of (7*S*,8*R*)-18-(benzyloxy)-8-chloro-2-methyloctadec-5-yn-7-ol (24)

To a cold (-78 °C), stirred solution of 5-methyl-1-hexyne (**23**) (1 g, 10.4 mmol) in dry THF (35 mL), a solution of *n*-butyllithium (2.5 M in hexanes, 3.75 mL, 9.37 mmol) was added dropwise. The resulting mixture was stirred at -78 °C for 45 minutes. After this time, a solution of (*R*)-12-(benzyloxy)-2-chlorododecanal (**22**) (1.71 g, 5.208 mmol) in THF (5 mL) was added dropwise and the reaction mixture was stirred for an additional 45 minutes. Then the reaction mixture was quenched with a saturated aqueous solution of NH_4Cl (20 mL), diluted with ethyl acetate (50 mL) and water (20 mL). The phases were separated, and the aqueous phase was extracted with ethyl acetate (3×50 mL). The combined organic layers were washed with brine (100 mL), dried over Na_2SO_4, and concentrated under reduced pressure, which afforded crude product (d.r. 20:1 determined by ^{1}H NMR analysis of the crude reaction mixture). Purification of the crude product by flash chromatography afforded (silica gel, 95:10 hexanes: ethyl acetate) (7*S*,8*R*)-18-(benzyloxy)-8-chloro-2-methyloctadec-5-yn-7-ol (**24**) (1.64 g, 68.3%). ^{1}H NMR (500 MHz, $CDCl_3$) δ: 7.36-7.32

(m, 5H), 4.53-4.49 (s, 3H), 4.04-3.97 (ddd, J = 9.4, 4.5, 3.5 Hz, 1H), 3.48-3.45 (d, J = 6.6 Hz, 2H), 2.29-2.19 (td, J = 7.4, 2.0 Hz, 2H), 1.89-1.75 (m, 2H), 1.72-1.56 (m, 6H), 1.36-1.24 (m, 17H), 0.9-0.88 (d, J = 6.7 Hz, 6H). ^{13}C NMR (125 MHz, $CDCl_3$) δ 138.59, 128.24, 127.53, 127.37, 87.74, 76.60, 72.76, 70.41, 67.52, 66.20, 37.26, 33.49, 29.67, 29.46, 29.38, 29.29, 27.17, 27.00, 26.39, 26.10, 22.07, 22.01, 16.65, 16.60. IR (neat): 3461, 2927, 2855, 2223, 1275, 713, 649 cm^{-1}. GCMS (EI) m/z calculated for $C_{26}H_{41}ClO_2$ $[M]^{+\cdot}$: 420.28; found: 421.20 $[\alpha]^{25}{}_D$: + 9.8 (c 1.54, $CHCl_3$).

Preparation of (7*R*,8*R*)-18-(benzyloxy)-8-chloro-2-methyloctadec-5-yn-7-yl benzoate (26)

To a cold (0 °C), stirred solution of (7*S*,8*R*)-18-(benzyloxy)-8-chloro-2-methyloctadec-5-yn-7-ol (**24**) (1.64 g, 3.88 mmol) and triphenylphosphine (2.03 g, 7.763 mmol) in dry THF (30 mL) under N_2 atmosphere, benzoic acid (**25**) was added (0.947 g, 7.763 mmol). The mixture was stirred 10 min. at same temperature and then DIAD (Diisopropyl azodicarboxylate) (1.35 g, 7.763 mmol) was added dropwise. After, the reaction mixture was stirred for 16 h at room temperature. Then the solvent (THF) was removed by rotovap and the crude was purified by flash column chromatography (silica gel, 95:5 hexanes: ethyl acetate) to afford (7*R*,8*R*)-18-(benzyloxy)-8-chloro-2-methyloctadec-5-yn-7-yl benzoate (**26**) (1.52 g, 74%). ^{1}H NMR (500 MHz, $CDCl_3$) δ: 8.14-8.09 (m, 2H), 7.52-7.45 (m, 3H), 7.37-7.32 (m, 5H), 4.51-4.50 (s, 3H), 4.04-3.99 (m, 1H), 3.48-3.45 (t, J = 6.7 Hz, 2H), 2.27-2.21 (td, J = 7.4, 2.0 Hz, 3H), 1.89-1.74 (m, 3H), 1.71-1.55 (m, 5H), 1.35-1.25 (s, 16H), 0.91-0.89 (d, J = 6.6 Hz, 6H). ^{13}C NMR (125 MHz, $CDCl_3$) δ: 171.85, 138.57, 133.76, 133.64, 130.20, 130.05, 129.23, 128.45, 128.36, 128.26, 127.56, 127.40, 87.81, 76.57, 72.76, 70.42, 67.52, 67.26, 66.23, 37.27, 33.51, 29.67, 28.98, 27.18, 27.02, 22.08, 22.03, 16.62. IR (neat): 2926, 2854, 2249, 1729, 1263, 1103, 734, 710 cm^{-1}. GCMS (EI) m/z calculated for $C_{33}H_{45}ClO_3$ $[M]^{+\cdot}$: 524.31; found: 524.20 $[\alpha]^{25}{}_D$: + 11.3 (c 1.38, $CHCl_3$).

Preparation of (7*R*,8*R*)-8-chloro-18-hydroxy-2-methyloctadecan-7-yl benzoate (27)

To a stirred solution of (7*R*,8*R*)-18-(benzyloxy)-8-chloro-2-methyloctadec-5-yn-7-yl benzoate (**26**) (0.8 g, 1.526 mmol) in methanol (20 mL) at room temperature, 10% Pd/C (80 mg) was added. The reaction mixture was hydrogenated under balloon pressure for 12 h. Pd/C was removed by filteration and rinsing with 10% MeOH/ CH_2Cl_2 (3×20 mL). Then the pooled filtrate was evaporated under reduced pressure to afford the crude product. The crude was purified by flash column chromatography (silica gel, 95:5 hexanes: ethyl acetate) to yield (7*R*,8*R*)-8-chloro-18-hydroxy-2-methyloctadecan-7-yl benzoate (**27**) (0.591 g, 88%). ^{1}H NMR (500 MHz, $CDCl_3$) δ: 8.10-8.07 (d, *J* = 7.4 Hz, 2H), 7.60-7.55 (d, *J* = 7.4 Hz, 1H), 7.47-7.44 (m, 2H), 5.33-5.26 (dt, *J* = 7.4, 3.1 Hz, 1H), 4.09-4.02 (dt, *J* = 7.2, 3.2 Hz, 1H), 3.72-3.59 (s, 2H), 1.88-1.81 (s, 2H), 1.79-1.71 (d, *J* = 38.7 Hz, 2H), 1.62-1.54 (s, 3H), 1.52-1.47 (s, 1H), 1.37-1.24 (m, 19H), 0.86-0.83 (d, *J* = 6.6 Hz, 6H). ^{13}C NMR (125 MHz, $CDCl_3$) δ: 165.91, 130.07, 129.87, 129.77, 129.61, 128.36, 128.30, 75.63, 63.87, 62.90, 38.63, 34.45, 32.59, 31.32, 29.39, 29.26, 28.89, 27.84, 27.68, 27.08, 26.53, 25.70, 25.60, 25.55, 22.51, 22.48. IR (neat): 3446, 2926, 2855, 1721, 1268, 1109, 1069, 1026, 711 cm^{-1}. GCMS (EI) m/z calculated for $C_{26}H_{43}ClO_3$ $[M]^{+\cdot}$: 438.29; found: 438.20 $[\alpha]^{25}{}_D$: + 10.9 (c 1.52, $CHCl_3$).

Preparation of (11*S*,12*R*)-11,12-epoxy-17-methyl-octadecan-1-ol (4)

To a stirred solution of (7*R*,8*R*)-8-chloro-18-hydroxy-2-methyloctadecan-7-yl benzoate (**27**) (0.55 g, 1.254 mmol) in methanol (4 mL) at room temperature, 4N NaOH (4 mL) was added. This reaction mixture was stirred for 2h. After this time, the solvent was removed by roto evaporation. The resulting residue was diluted with ethyl acetate (50 mL) and water (15 mL). The phases were separated, and the aqueous phase was extracted with ethyl acetate (3×20 mL). The combined organic layers were washed with brine (50 mL), dried over Na_2SO_4, and concentrated under reduced pressure, which afforded crude product. The crude material purified by flash column chromatography (silica gel, 95:5 hexanes: ethyl acetate) to yield (11*S*,12*R*)-11,12-epoxy-17-methyl-octadecan-1-ol (**4**) (0.308 g, 82%). ^{1}H NMR (500 MHz, $CDCl_3$) δ: 3.67-3.61 (t, *J* = 6.6 Hz, 2H), 2.95-2.86 (m, 2H), 1.63-1.46 (m,

10H), 1.40-1.26 (m, 17H), 0.89-0.85 (d, J = 6.6 Hz, 7H). ^{13}C NMR (125 MHz, $CDCl_3$) δ: 62.98, 57.16, 38.80, 32.70, 29.45, 29.43, 29.36, 29.30, 27.80, 27.76, 27.72, 27.22, 26.76, 26.50, 25.62, 22.52, 22.51. IR (neat): 3404, 2924, 2854, 1366, 1267, 1095, 1058 cm^{-1}. GCMS (EI) m/z calculated for $C_{19}H_{38}O_2$ $[M]^{+\cdot}$: 298.29; found: 298.30 $[\alpha]^{25}{}_D$: + 5.7 (c 1.5, $CHCl_3$).

Preparation of 2-(2-(prop-2-yn-1-yloxy)ethoxy)acetic acid (30), Scheme S1

Diethylene glycol (**28**) (1.5 g, 14.15 mmol) was dissolved in anhydrous THF (50 mL) in a round bottom flask. To this homogeneous solution, NaH was added (0.34 g, 1415 mmol) at 0°C under inert atmosphere. After half an hour of stirring, the propargyl bromide (**29**) (1.18 g, 14.15 mmol) was added dropwise to the flask and the mixture was stirred at room temperature for 16h. Then the reaction was poured into the ice-cold water and diluted with EtOAc (50 mL). The aqueous layer was separated and extracted with ethyl acetate (2×50 mL). The combined organic layers were washed with brine solution (50 mL), dried over Na_2SO_4, and concentrated under reduced pressure, which afforded crude product. The crude product was purified through flash column chromatography (silica gel, 80: 20 hexanes: ethyl acetate) to yield 2-(2-(prop-2-yn-1-yloxy) ethoxy) ethan-1-ol (**30**) (1.1 g, 54%). ^{1}H NMR (500 MHz, $CDCl_3$) δ: 4.08-4.04 (d, J = 2.4 Hz, 2H), 3.59-3.51 (m, 6H), 3.46-3.43 (m, 2H), 3.27-3.20 (s, 1H), 2.41-2.36 (t, J = 2.4 Hz, 1H). ^{13}C NMR (125 MHz, $CDCl_3$) δ: 79.06, 74.39, 72.13, 69.61, 68.58, 61.00, 57.84. IR (neat): 3288, 2924, 2857, 2117, 1066, 1045cm^{-1}. GCMS (EI) m/z calculated for $C_7H_{12}O_3$ $[M\text{-}C_3H_4]$: 104.06; found: 104.10.

To a stirred solution of 2-(2-(prop-2-yn-1-yloxy) ethoxy) ethan-1-o l (**30**) (0.3 g, 2.083 mmol) in acetone (10 mL) at 0° C 10 % $NaHCO_3$ solution was added. The reagent 2, 2, 6, 6-Tetramethylpiperidin-1-yl (TEMPO, 0.358 g, 2.283 mmol) was added to the heterogeneous reaction mixture followed by KBr (0.0024 g, 0.283 mmol). After that, sodium hypochlorite (NaOCl, 10% solution, 1.95 mL, and 2.625mmol) was added dropwise at 0° C, and the reaction mixture was stirred at room temperature for 16h. The reaction mixture was diluted with H_2O (10 mL) and EtOAc (50 mL). The organic and aqueous layers were separated, and the aqueous layer was extracted with ethyl acetate

(2×10 mL). All the organic layers were combined, washed with saturated NaCl solution, dried over Na_2SO_4 and concentrated in *vacuo*. After, the residue was purified by flash chromatography (silica gel, 80: 20 hexanes: ethyl acetate) it yielded 2-(2-(prop-2-yn-1-yloxy)ethoxy)acetic acid (**5**) (0.298 g, 90%). ^{1}H NMR (500 MHz, $CDCl_3$) δ: 7.92 (s, 2H), 4.21-4.15 (m, 4H), 3.78-3.70 (m, 4H), 2.45 (t, *J* = 2.3 Hz, 1H). ^{13}C NMR (125 MHz, $CDCl_3$) δ: 174.26, 79.02, 75.01, 74.80, 70.69, 68.77, 68.17, 58.29. IR (neat): 2989, 2925, 2857, 2117, 1729, 1249, 1094 cm^{-1}. GCMS (EI) m/z calculated for $C_7H_{10}O_4$ [M-C_3H_4]: 118.03; found: 118.10.

Preparation of 10-((2*S*,3*R*)-3-(5-methylhexyl)oxiran-2-yl)decyl 2-(2-(prop-2-yn-1-yloxy)ethoxy)acetate (31)

To a stirred solution (11*S*,12*R*)-11,12-epoxy-17-methyl-octadecan-1-ol (**4**) (0.1 g, 0.3355 mmol) in dichloromethane (5 mL), 2-(2-(prop-2-yn-1-yloxy) ethoxy) acetic acid (**5**) (0.107 g, 0.6711 mmol) was added at room temperature. Then *N*,*N'*-diisopropylcarbodiimide-(DIC, 0.845 g, 0.6711 mmol) and *N*,*N*-dimethyl-4-aminopyridine (DMAP, 8.2 mg, 0.0671 mmol) were added, and the resulting homogeneous reaction mixture was stirred at room temperature for overnight. The dichloromethane solvent that was removed under reduced pressure afforded oily residue, which after column purification by flash chromatography (silica gel, 95:5 hexanes: ethyl acetate) yielded 10-((2*S*, 3*R*)-3-(5-methylhexyl) oxiran-2-yl) decyl 2-(2-(prop-2-yn-1-yloxy) ethoxy) acetate (**31**) (0.114 g, 78%). ^{1}H NMR (500 MHz, $CDCl_3$) δ: 4.24-4.19 (d, *J* = 2.4 Hz, 2H), 4.17-4.12 (m, 4H), 3.79-3.71 (m, 4H), 2.94-2.86 (m, 2H), 2.45-2.41 (t, *J* = 2.4 Hz, 1H), 1.67-1.61 (m, 2H), 1.55-1.45 (m, 7H), 1.40-1.24 (m, 18H), 0.89-0.86 (d, *J* = 6.6 Hz, 6H). ^{13}C NMR (125 MHz, $CDCl_3$) δ: 170.35, 79.37, 74.50, 70.56, 68.99, 68.54, 64.87, 58.27, 57.11, 38.78, 29.41, 29.33, 29.08, 28.45, 27.77, 27.74, 27.70, 27.20, 26.74, 26.50, 25.71, 22.50, 22.49. IR (neat): 2925, 2855, 2115, 1752, 1203, 1146, 1103 1032 cm^{-1}. GCMS (EI) m/z calculated for $C_{26}H_{46}O_5$ [M+1]: 438.33; found: 439.30 $[\alpha]^{25}{}_D$: + 3.7 (c 0.5, $CHCl_3$).

HPLC method for separating enantiomers of epoxy phenyltriazoles 35, 36 and *ent*-36

The resulting triazoles **35**, **36** and *ent*-**36** are UV absorbing compounds, which are amenable to separation by HPLC and detection by variable wavelength detector (VWD). The scalemic triazole **35** was separated by chiral HPLC using a chiral column (Phenomenex Lux 5μm Cellulose-2). The flow rate was set to be 0.2 mL/min. The solvent system IPA/hexane/DEA used as eluent. The enantiopure triazoles **36** and *ent*-**36** were eluted at 5.55 min and 6.56 min, respectively (Fig. 2). The enantiomeric excess of epoxy alkyne **31** and *ent*-**31** was determined to be greater than 98%.

Preparation of fluorescently tagged (+)-disparlure (1a)

In a 2 mL reaction vial, 6-FAM azide **32** (1 mg, 0.0022 mmol) and 10-((2*S*,3*R*)-3-(5-methylhexyl)oxiran-2-yl)decyl 2-(2-(prop-2-yn-1-yloxy)ethoxy)acetate (**31**) (5 mg, 0.0114 mmol) were added to the mixture of tris(3-hydroxypropyltriazolylmethyl)amine (THPTA, 1 mg, 0.0023 mmol) sodium ascorbate (28 mg, 0.01144 mmol), and copper (II) sulfate heptahydrate (1.1 mg, 0.0057 mmol) dissolved in ratio of 1:1 volume of *t*-BuOH and water (1 mL) at room temperature. The reaction mixture was stirred at room temperature for 1h. After this time, the t-BuOH was removed, and the resulting residue was diluted with water and dichloromethane. The aqueous layer was extracted with 10% MeOH/DCM (4×10 mL). The pooled organic layers were washed with saturated sodium chloride solution, dried over Na_2SO_4 and concentrated *in vacuo*. The crude residue was purified by column chromatography on neutral alumina (10% MeOH/CH_2Cl_2) yielded 6-FAM tagged (+)-disparlure **1a** (1.12 mg, 57.4%). ^{1}H NMR (600 MHz, $CDCl_3$) δ: 8.17-8.07 (m, 4H), 8.07 (s, 1H), 7.63 (s, 2H), 6.73-6.53 (m, 6H), 4.79 (s, 2H), 4.18-4.08 (m, 4H), 3.78 (td, *J* = 5.4, 3.5 Hz, 4H), 3.41 (t, *J* = 6.9 Hz, 2H), 3.36 (t, *J* = 6.7 Hz, 2H), 2.90 (t, *J* = 3.9 Hz, 2H), 1.82 (p, *J* = 6.8 Hz, 2H), 1.63 (dt, *J* = 13.7, 6.7 Hz, 4H), 1.54-1.45 (m, 7H), 1.38-1.22 (m, 17H), 0.87 (d, *J* = 6.6 Hz, 6H). IR (neat): 3570-3245 (O-H & N-H str), 2924-2856 (C-H str), 1771, 1749, 1690, 1625, 1591, 1524, 1456, 1439, 1250, 1213, 1148, 1104 1029 cm^{-1}. HRMS (ESI) m/z calculated for $C_{50}H_{65}N_4O_{11}$ [M+H]: 897.4650; found: 897.4662.

Determination of Quantum Yield (Φ) and Molar Extinction Coefficient (ε) for 6-FAM (+)-disparlure (1a)

In order to determine the quantum yield (Φ) for the 6-FAM (+)-disparlure (**1a**), the 6-FAM azide was used as reference fluorophore as it has the same excitation and emission wavelengths as the 6-FAM (+)-disparlure. The quantum yield of 6-FAM azide is 0.90 at the excitation wavelength of 494 nm. In this experiment, the solutions of the reference and the sample (6-FAM (+)-disparlure) with the absorbance values from 0.01 to 0.04 were considered to minimize the fluorescence inner-filter effect (IFE). A series of four standard solutions in phosphate buffer or 1-heptanol were prepared each for 6-FAM (+)-disparlure and 6-FAM azide, with the absorbance values between 0.01 to 0.04. The absorption spectra of these solutions were recorded on VWR UV-6300PC double beam spectrophotometer (VWR, PA, USA) at excitation wavelength of 494 nm. The fluorescence emission spectra of both reference and samples solutions were recorded on fluorescent spectrophotometer (PTI-QunataMaster) over the wavelength range 450 to 600 nm at excitation wavelength 494 nm. The plots of integrated fluorescence intensity of the emission spectra against the absorbance of the both 6-FAM azide and 6-FAM (+)-disparlure showed a linear relationship (Fig. S7, supporting information). The slope of the liner fit for the 6-FAMazide and 6-FAM (+)-disparlure is used to calculate the quantum yield (Φ) of 6-FAM (+)-disparlure according to the equation below.

$$\Phi_{FD} = \Phi_{FA} \, (m_{FD}/m_{FA}) \, (\eta^2_{FD}/\eta^2_{FA}) \quad \text{(Eq. 1)}$$

Where Φ_{FD} is the quantum yield of 6-FAM (+)-disparlure, Φ_{FA} is the quantum yield of the 6-FAM azide (standard), m_{FD} and m_{FA} are the slope of the linear fit for the 6-FAM (+)-disparlure and 6-FAM azide, respectively, and η^2_{FD} and η^2_{FA} are the refractive indices of the 6-FAM (+)-disparlure and 6-FAM azide solutions, respectively. Since the same buffer was used for both fluorophores, the term $\eta^2_{FD}/\eta^2_{FA} = 1$ and we get:

$$\Phi_{FD} = \Phi_{FA} \, (m_{FD}/m_{FA}) \quad \text{(Eq. 2)}$$

To determine the molar extinction coefficient (ε) for 6-FAM (+)-disparlure **1a**, a series of four sample solutions was prepared by diluting the 6-FAM (+)-disparlure in phosphate buffer (pH 8) or 1-heptanol. The absorption spectra for these solutions were recorded on UV/vis spectrophotometer at excitation wavelength of 494 nm. The plot of concentration

of 6-FAM (+)-disparlure against the absorbance showed a linear relationship (Fig. S8, supporting information). According to the Beer-Lambert law (A = εbc), where b is the path length of the cuvette which is equal to 1 in most instances. Therefore, the slope of absorbance (A) vs concentration plot is equal to the molar extinction coefficient.

Fluorescence Binding Assay

To determine the binding affinity of disparlure enantiomers to pheromone binding proteins (*Ldis* PBP1 and *Ldis* PBP2), fluorescence binding assays were conducted on a fluorescent spectrophotometer (PTI-QuantaMaster) using 6-FAM tagged-disparlure enantiomers **1a** and *ent*-**1a** as fluorescent probes. The fluorescence spectra were recorded at room temperature with a silica quartz cuvette (light path = 1 cm). The protein (0.04 μm), *Ldis*PBP1 or *Ldis*PBP2 in 50 mM phosphate buffer (pH 8.0) was titrated with fluorescent probes **1a** or *ent*-**1a** to final concentrations 2- 60 nM. The complex between the fluorescent probe and *Ldis*PBPs was excited at 494 nm and the fluorescence emission spectra were monitored between 450 to 600 nm.

To measure the dissociation constant (K_d) of the complex, the values of fluorescent intensity of fluorescent probes at the emission maximum (after buffer and protein background correction) were plotted against total fluorescent probe concentrations and the data were fitted into nonlinear regression model (curve fit) using GraphPad Prism 5 (GraphPad Software LLC). To determine the K_d for the competitor ligands, (+)-disparlure (**1**) and (-)-disparlure (*ent*-**1**) the competitive binding assay was performed. Aliquots of the competitor ligand in ethanol were added to the solution containing 0.04 μM (40 nM) protein and fixed concentration of fluorescent probe (60 nM). A decrease in the relative fluorescence intensity suggested that the competitor removed the fluorescent probe from the binding site of the protein. The inhibitory constant (K_i), was calculated based on the competitor IC_{50} value using the following equation:

$$K_i = [IC_{50}]/1 + [F]/K_{dF}, \qquad \text{(Eq. 3)}$$

where [F] is the total fluorescent probe concentration and K_{dF} is the binding constant of the fluorescent probe to the *Ldis*PBPs. The dissociation constant of the ligand (K_{dL}, see Eq. 4 below) can then be obtained as follows. The equilibrium between P.F (the protein – fluorescent probe complex), L (the ligand of interest) and F (the fluorescent reporter) is:

$$P.F + L \leftrightarrow P.L + F$$

$$K_i = [P.F][L]/[P.L][F] \quad \text{(Eq. 4)}$$

The equilibria between the probe and the protein, as well as the ligand and the protein are:

$$F + P \leftrightarrow P.F \quad K_{dF} = [P][F]/[P.F] \quad \text{(Eq. 5)}$$

$$L + P \leftrightarrow P.L \quad K_{dL} = [P][L]/[P.L] \quad \text{(Eq. 6)}$$

Substituting Eq. 5 and 6 into Eq. 4, we get:

$$K_i \times K_{dF} = K_{dL} \quad \text{(Eq. 7)}$$

Results

Design of 6-FAM-tagged disparlure enantiomers

Herein, we describe the design and convergent synthesis of 6-carboxyfluorescein (6-FAM)-tagged (+)-disparlure analogue (**1a**) taking advantage of the copper (I)-catalyzed Huisgen 1,3-dipolar cycloaddition (also known as click reaction). The target molecule has been divided into three parts: (+)-disparlure (**1**) (pheromone, recognition part) for the selective binding towards its pheromone binding protein, 6-FAM moiety for the fluorescence detection, and finally between the two parts, a diethylene glycol linker to increase the hydrophilicity of the final target molecule and provide some separation between the recognition part and the fluorophore (Scheme. 1).

The design for 6-FAM (+)-disparlure (**1a**) is outlined in Scheme 1. We believed that the target molecule **1a** could be prepared by the click reaction between the 6-carboxyfluorescein azide (6-FAM azide) **2** and epoxy alkyne intermediate **3** which could be assembled by esterification of epoxy alcohol **4** and the alkyne acid **5**. The retrosynthetic analysis of epoxy alcohol fragment **4** reveals that this could be synthesized from1,2-*syn* chlorohydrin **6** which could be obtained by Mitsunobu inversion of 1,2-*anti* chlorohydrin **7**. We envisioned that the stereocenter at carbon-8 of 1,2-*anti* chlorohydrin **7** could be introduced by utilizing a diastereoselective nucleophilic addition reaction between enantiopure α-chloroaldehyde **8** and acetylide anion. The enantiopure α-chloroaldehyde **8** could be prepared from aldehyde intermediate **10** via asymmetric α-chlorination. We used the same approach to prepare (+)- and (-)-disparlure enantiomers (Pinnelli et al. 2019). The asymmetric α-chlorination of an aldehyde was also used previously in the synthesis of the posticlure enantiomers, which have a *trans* epoxide moiety (Kang and Britton 2007). To obtain the *cis* epoxide of disparlure we had to invert the configuration of the intermediate anti chlorohydrin (Pinnelli et al. 2019).

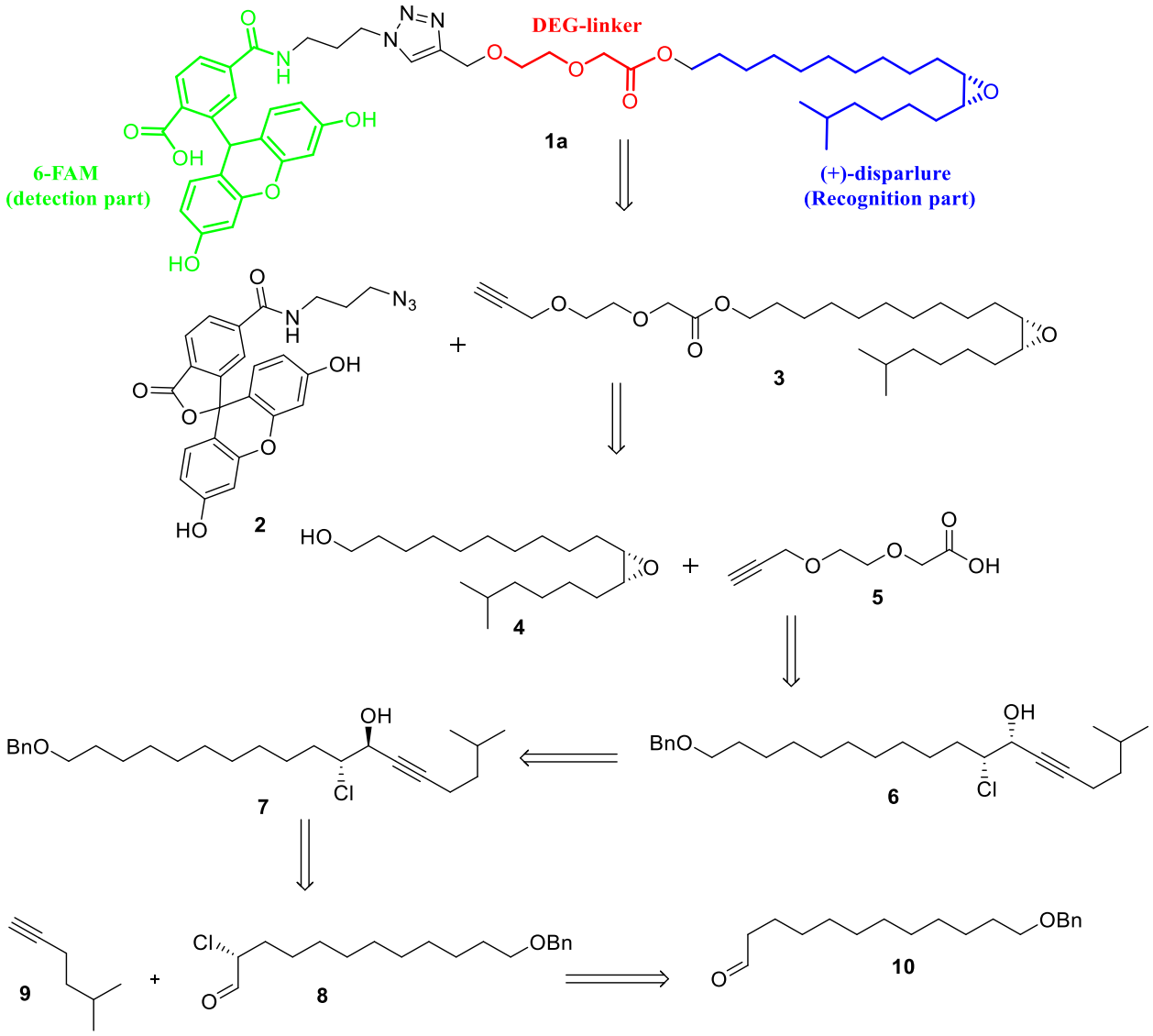

Scheme. 1. Retereosynthetic design for 6FAM-tagged (+)-disparlure (**1a**).

*Synthesis of key fragment, enantiopure cis-epoxy alcohol **4***. To accomplish the synthesis of the 6-FAM (+)-disparlure (**1a**), two key fragments (*i.e.*, enantiopure *cis*-epoxy alcohol **4** and ethylene glycol linker **5** have been prepared and their synthetic routes are discussed below. The first task of the synthesis was the preparation of enantiopure epoxy alcohol fragment **4**, which began from commercially available 1,12-dodecanediol (**11**) (Scheme 2). The diol **11** was treated with chloromethyl methyl ether (MOM-Cl) or tert-Butyldimethylchlorosilane (TBDMS-Cl) to afford the mono MOM or TBDMS protected alcohol **12** or **13**.

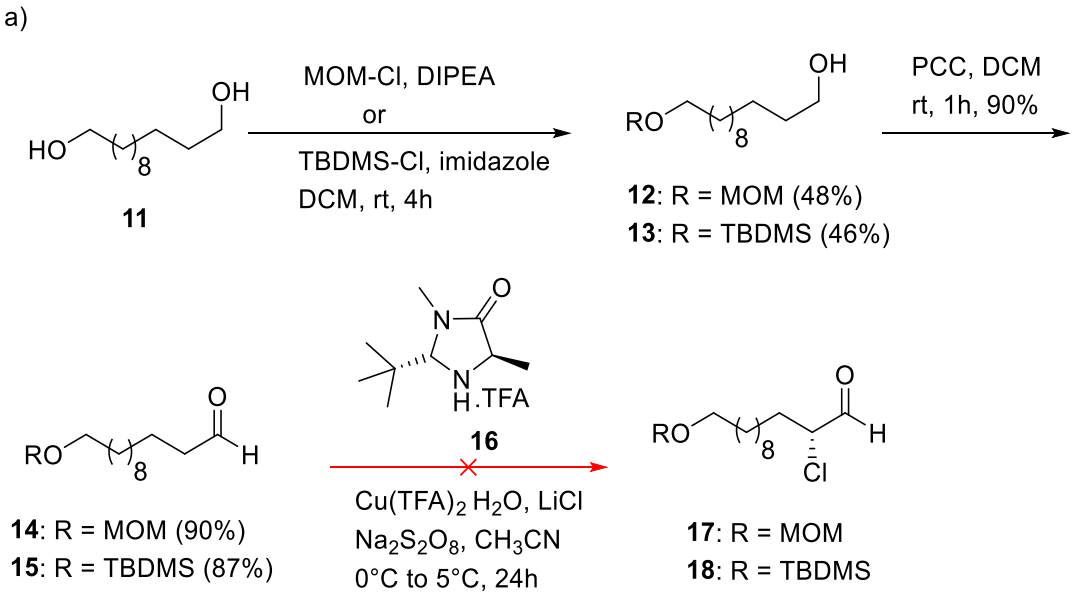

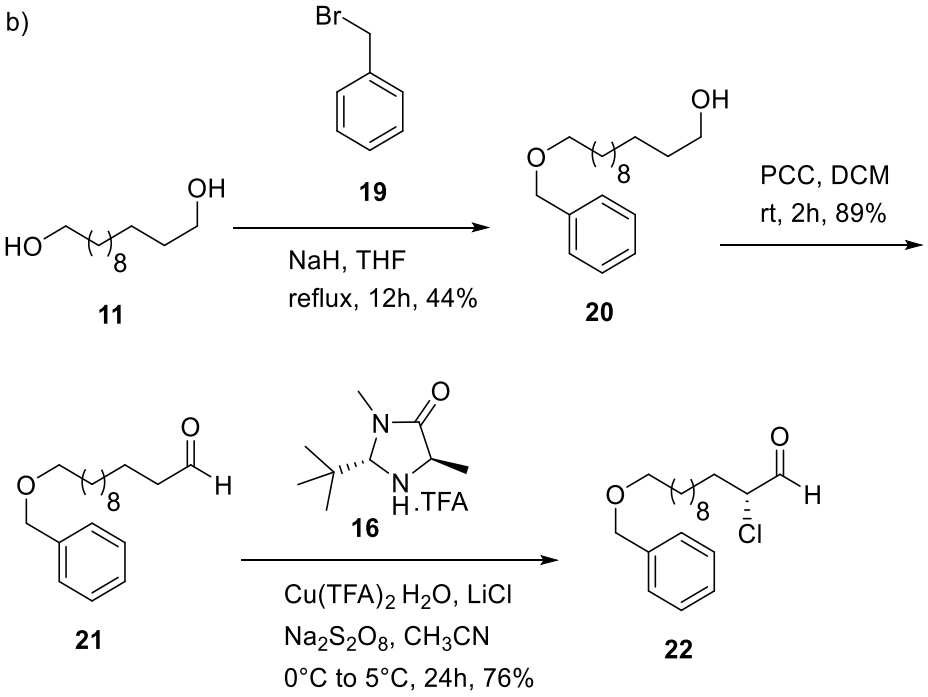

Scheme 2. a) Attempted asymmetric α-chlorination of MOM or TBDMS protected aldehyde with SOMO catalyst **16**. b) Synthesis of benzyl-protected enantiopure α-chloroaldehyde **22**.

Subsequent oxidation of compound **12** or **13** with pyridinium chlorochromate (PCC) furnished the aldehyde **14** or **15**. We attempted to asymmetrically chlorinate aldehydes **14** or **15**, using a previously reported asymmetric chlorination reaction (Amatore

et al. 2009; Pinnelli et al. 2019). In this reaction, chiral amine (2*R*,5*S*)-2-*tert*-butyl-3,5-dimethylimidazolidin-4-one (**16**) and LiCl are used as catalyst and chlorinating agent, respectively. However, this reaction gave a mixture of decomposition products and failed to provide the desired products **17** or **18** (Scheme 2). The ^{1}H NMR analysis of the crude product showed deprotection of the MOM or TBDMS groups leading to the formation of mixtures of decomposition products.

To overcome this problem, an alternative approach was employed in which benzyl protecting group was utilized during protection of the diol **11**. The monobenzylated alcohol **20** was prepared by benzylation of diol **11** with benzylbromide **19** in the presence of NaH/THF at 70°C (Scheme 2b). ^{1}H NMR analysis of the crude reaction mixture indicated approximately 1:1 ratio of mono and dibenzylated products. Upon purification by flash column chromatography, 44% yield of the monobenzylated alcohol **20** was isolated. The resulting monobenzylated alcohol **20** was oxidized with PCC under standard conditions to its corresponding aldehyde **21**, followed by asymmetric α-chlorination with SOMO catalyst **16** to afford enantiopure α-chloroaldehyde **22** in 85% yield and >98% ee (Fig. S4, supporting information). With the required enantiopure α-chloroaldehyde **22**, we proceeded to prepare the 1,2-*anti* chlorohydrin **24** as shown in Scheme 3. Previous studies have shown that addition of a nucleophile to a chiral α-chloroaldehyde delivers predominantly 1,2-*anti*-chlorohydrin (Kang and Britton 2007; Shibuya et al. 2008; Pinnelli et al. 2019). Therefore, the 5-methyl-1-hexyne (**23**) was treated with *n*-butyllithium followed by slow addition of enantiopure α-chloroaldehyde **22** to afford 1,2-*anti* chlorohydrin **24**. ^{1}H NMR data of the crude reaction mixture revealed a diastereomeric ratio (d.r) of ~ 20:1 (*anti*:*syn*). The crude reaction mixture was subjected to column chromatography yielding the 1,2-*anti* chlorohydrin **24** as pale-yellow oil in 68% yield.

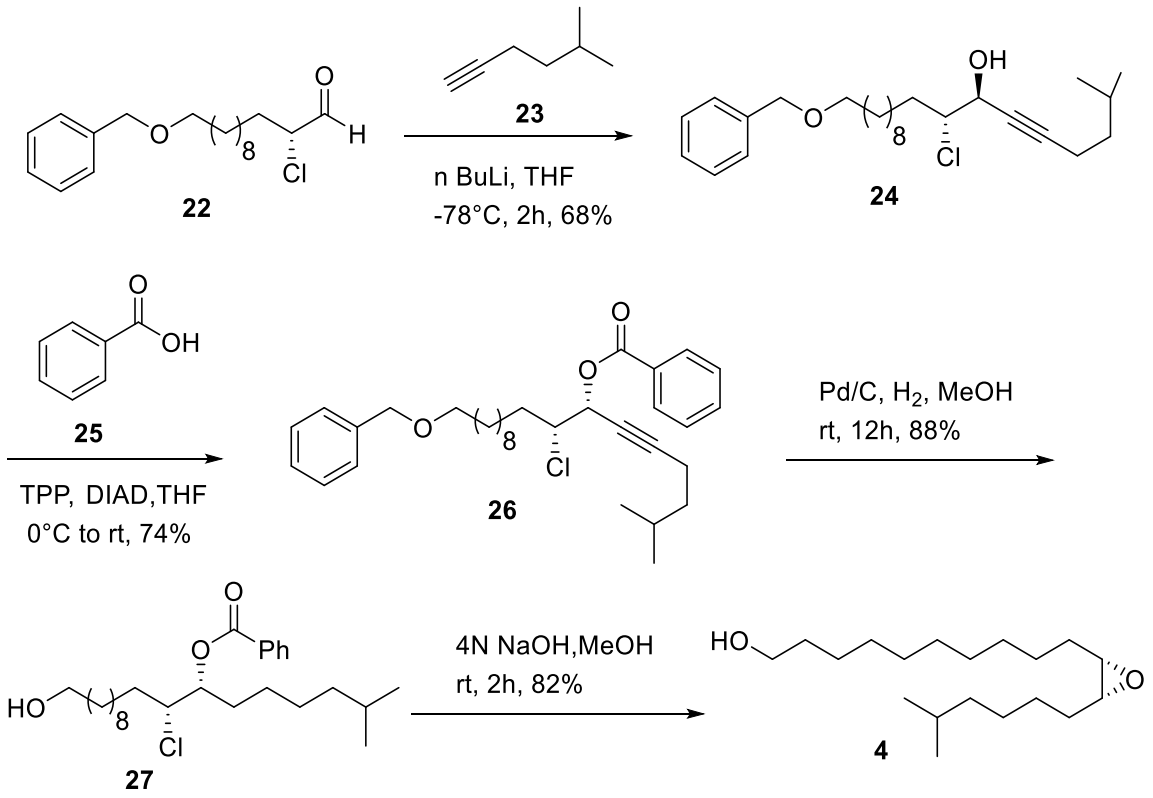

Scheme 3. Syntheis of key fragment epoxy alcohol **4**.

We required a 1,2-*syn* chlorohydrin to obtain the key intermediate epoxy alcohol **4**. Therefore, the stereochemistry at the C-8 carbon of 1,2-*anti* chlorohydrin **24** was inverted under Mitsunobu conditions (Scheme 3). Compound **24** was treated with benzoic acid (**25**), tri-phenylphosphine (TPP) and diisopropyl azadicarboxylate (DIAD) in dry THF under an inert atmosphere. This resulted in the completely inverted product **26**, which was obtained in 80% yield. Then, a one-pot deprotection of the benzyl group and alkyne reduction of the 1,2-*syn* chloroester **26** was carried out, using 10% Pd/C in MeOH in the presence of hydrogen (1 atm, balloon). Thus, formation of compound **27**, using Pd/C and followed by basic hydrolysis of benzoate of 1,2-*syn* chloroester **27**, led to the key fragment, enantiopure *cis*-epoxy alcohol **4** in good yield (Scheme 3). The required ethylene glycol linker **5** for esterification of enantiopure epoxy alcohol **4** was prepared by the synthetic pathway shown in Scheme S1 (supporting information).

*Synthesis of 6FAM-tagged disparlure enantiomers **1a** & **ent-1a***. Finally, the key fragments **4** and **5** were coupled under Steglich conditions, which involve DIC (*N*,*N*′-

diisopropylcarbodiimide) as coupling reagent and DMAP (*N*,*N*′-dimethylaminopyridine) as a catalyst, leading to the required alkyne ester **31** with good yield, thus building the appropriate alkyne partner for the click reaction employing 6-FAM azide as the coupling partner (Scheme 4). From alkyne **31**, the (+)-disparlure-based fluorescent probe was synthesized (Scheme 4). The alkyne **31** and 6-FAM azide **32** were subjected to the copper-catalyzed azide-alkyne cycloaddition using THPTA (tris(benzyltriazolylmethyl)amine), sodium ascorbate and copper (II) sulphate at room temperature. This reaction led to the desired (+)-disparlure fluorescent probe **1a** with 57% yield.

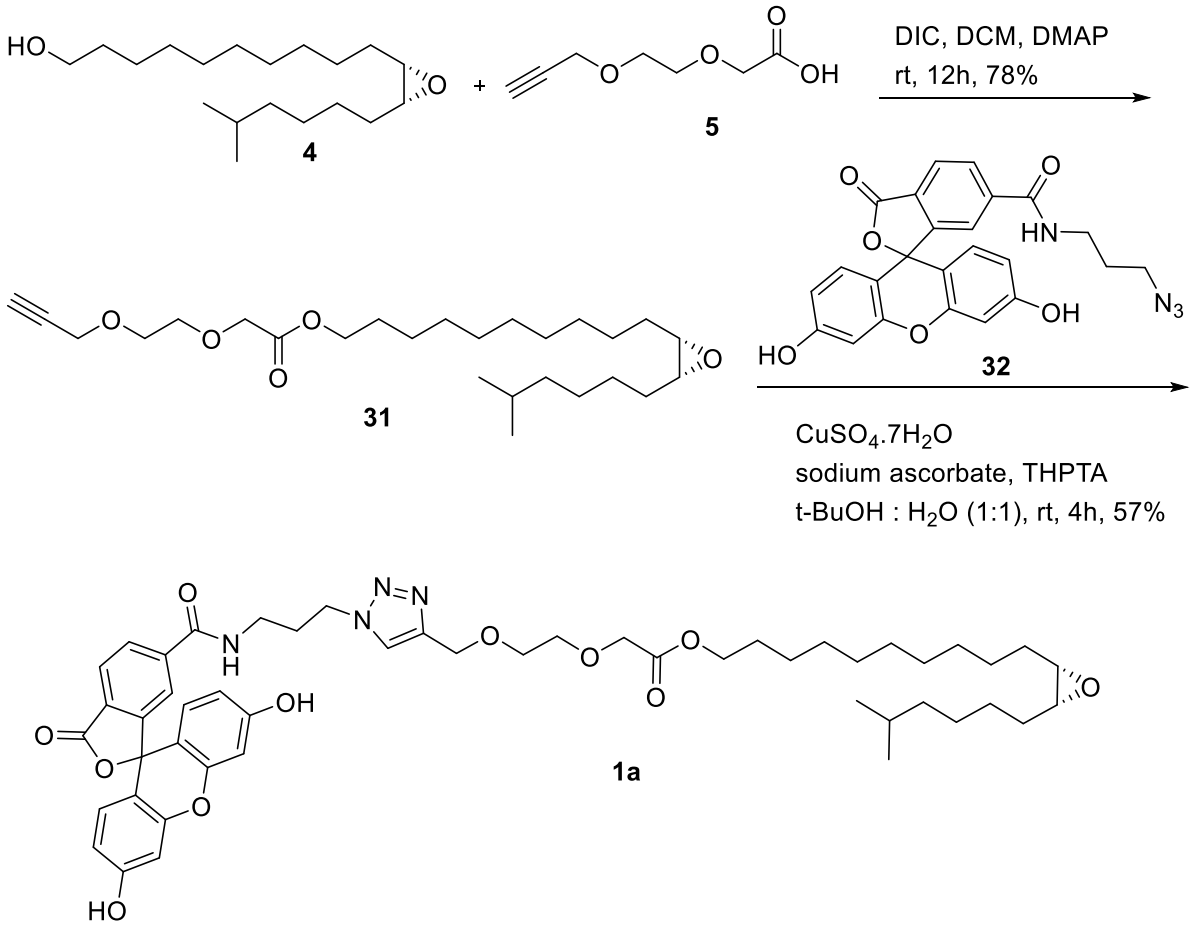

Scheme 4. Synthesis of 6-FAM-tagged-(+)-disparlure **1a**.

For the preparation of 6-FAM (-)-disparlure *ent*-**1a** (Scheme S2 & S3, see supporting information), the chiral amine catalyst *ent*-**16** (2R,5S)-2-(tert-butyl)-3,5-dimethylimidazolidin-4-one was used to synthesize α-chloroaldehyde *ent*-**22**.

Diastereoselective nucleophilic addition of *ent*-**22** with lithium alkyne afforded *ent*-**24** in good yield. Mitsunobu inversion of *ent*-**24** with DIAD and benzoic acid delivered 1,2-*anti* chlorohydrin *ent*-**26**, which is subjected to hydrogenation with Pd/C and hydrogen gas followed by basic hydrolysis to yield epoxy alcohol *ent*-**4**. Next, Steglich esterification between the resulting epoxy alcohol *ent*-**4** and acid **5** in the presence of DIC and catalytic amount of DMAP yielded the required alkyne intermediate *ent*-**31**, a key precursor for the click reaction. Finally, the alkyne partner *ent*-**31** was coupled with 6-FAM azide **32** under click reaction conditions to deliver 6-FAM tagged (-)-disparlure *ent*-**1a** (Scheme S3, supporting information).

*Determination of enantiomeric excess of epoxy alkynes **31** **ent-31***. In order to determine the enantiomeric excess for the target molecules 6-FAM (+)-disparlure **1a** and 6-FAM (-)-disparlure *ent*-**1a**, a scalemic sample of epoxy alkyne **33** (Fig. 2) was prepared by mixing nearly equal amounts of enantiopure epoxy alkynes **31** and *ent*-**31** (Scheme 4 and S3). This scalemic epoxy alkyne **33** was later subjected to the click reaction using 4-bromophenylazide (**34**) as coupling partner to give corresponding scalemic triazole **35**. Fig. 2 showed baseline separation of the scalemic triazole **35**, allowing us to determine the enantiomeric excess (*ee*) of the alkynes **31** and *ent*-**31**. On the other hand, the enantiopure epoxy alkynes **31** and *ent*-**31** were transformed to their corresponding triazoles **36** and *ent*-**36** using the same click reaction conditions as shown in Scheme S4 (supporting information). Both probes had > 98% ee (see Table 2).

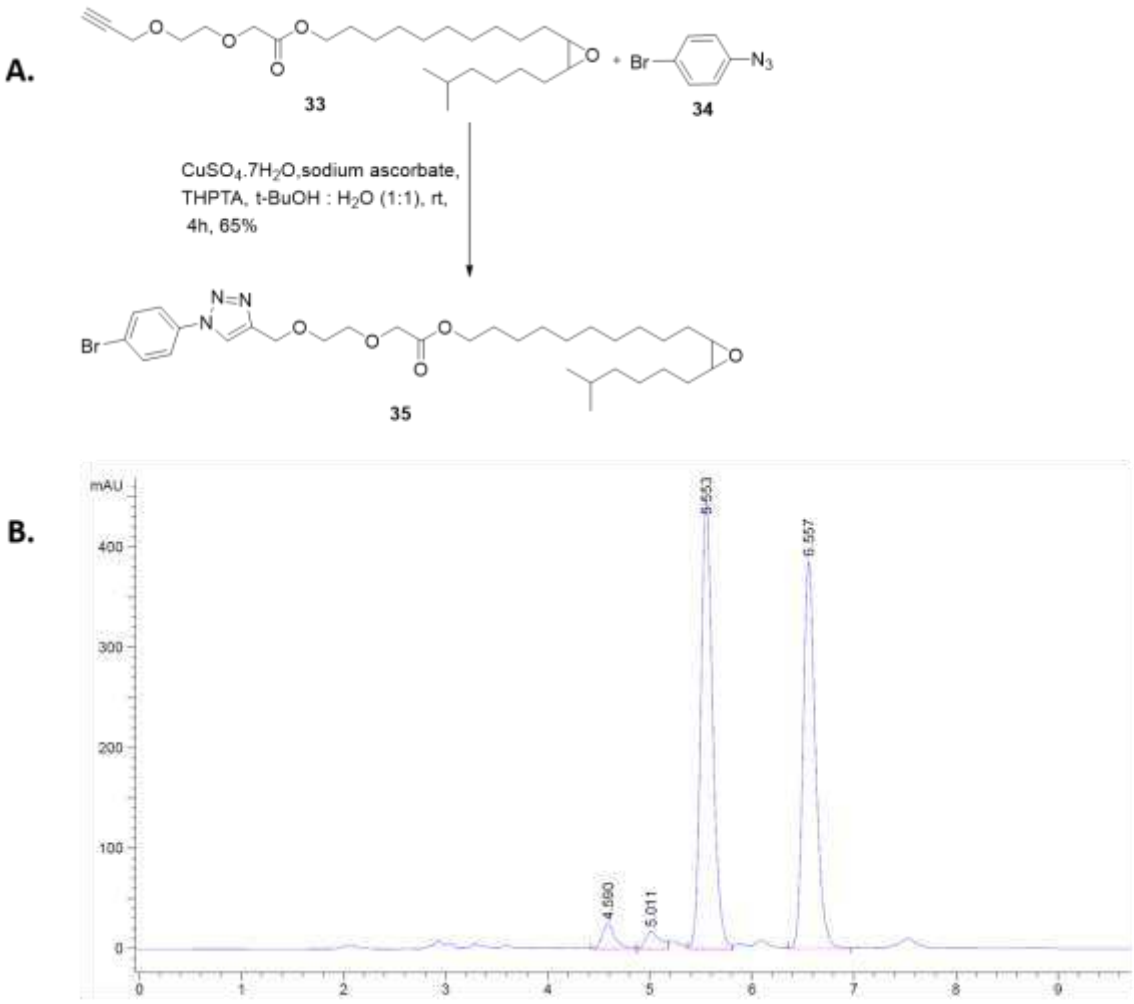

Figure 2. Determination of enantiomeric excess (*ee*) of epoxy alkynes 31 and *ent*-31 by forming of phenyltriazoles. **A** Reaction used to create the phenyltriazoles of scalemic disparlure with a linker. The major isomer that forms in the reaction is shown. **B** HPLC chromatogram of the resulting product.

*Characterization of 6-FAM (+)-disparlure **1a***. The absorbance and emission spectra of 6-FAM (+)-disparlure **1a** were recorded in phosphate buffer (pH 8) and 1-heptanol. A shift of 12 nm was noticed when comparing the excitation maximum of **1a** in 1-heptanol (λ_{max} 485) with that in phosphate buffer (λ_{max} 494) (see supporting information). The molar absorptivity (ε) of **1a** was determined in 1-heptanol ($\varepsilon_{485\ nm}$ = 3021 M^{-1} cm^{-1}) and in phosphate buffer ($\varepsilon_{497\ nm}$ = 16823 M^{-1} cm^{-1}) from absorption spectra recorded at different concentrations of **1a**. Compound **1a** shows maximal emission at 515 nm with a 30 nm Stokes shift and quantum efficiency of (Φ) 0.62 in 1-heptanol, whereas it exhibits

maximum emission at 520 nm with a Stokes shift of 26 nm and quantum efficiency of (Φ) 0.86 in phosphate buffer.

Table 1. Absorption and fluorescence properties of 6-FAM (+)-disparlure **1a** in phosphate buffer (pH 8).

λ_{ex} [nm]	λ_{em} [nm]	SS [nm]	$\varepsilon_{497\ nm}$ [M^{-1} cm^{-1}][b]	Φ[b]
494	520	26	$(16.8 \pm 0.3) \times 10^3$	0.86 ± 0.02

SS, Stokes shift; ε, molar extinction coefficient; Φ, quantum yield. [b] Values are reported ± standard error (SE) of 3 replicates.

Fluorescence emission of 6-FAM tagged disparlure enantiomers upon binding to LdisPBPs. We have examined the binding affinity of 6-FAM tagged disparlure enantiomers **1a** and *ent*-**1a** to *Ldis*PBP1 and *Ldis*PBP2 by fluorescence binding assay. When excited at 494 nm, fluorescent probes 6-FAM (+)-disparlure **1a** and 6-FAM (+)-disparlure *ent*-**1a** in phosphate buffer (pH 8) show a fluorescence emission with maximum at 520 nm. For example, Fig. 3A shows the emission spectra of fluorescent probe **1a** in phosphate buffer and in presence of *Ldis*PBP1. We can observe an increase in fluorescence emission intensity as fluorescent probe **1a** concentration increases (Fig. 3).

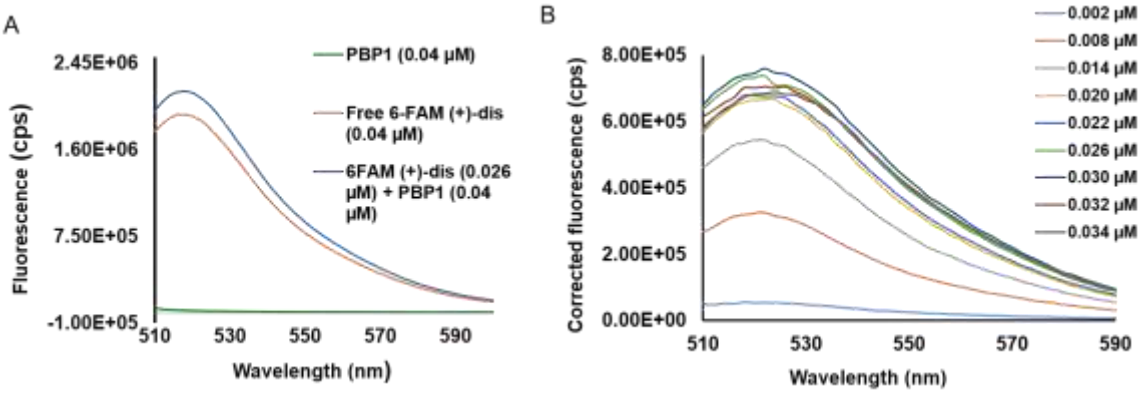

Figure 3. A 6-FAM (+)-disparlure **1a** emission spectra. **1a** bound to *Ldis*PBP1 was excited at 494 nm and its emission spectrum (blue trace) was recorded. The red trace shows the emission spectrum of 1a in buffer and the green trace shows the emission background obtained with only PBP in buffer. **B** Fluorescence emission spectra were recorded with increasing doses of 6-FAM (+)-disparlure **1a**, titrated into LdisPBP1.The fluorescence emission from 6-FAM (+)-disparlure **1a /** LdisPBP1 complex determined by substracting the bottom trace (red) from the upper trace (blue) in part **A**.

The increase in fluorescence intensity is a probable consequence of restricted rotation of the fluorophore upon binding to PBP. It has been reported that the fluorescent probes show week fluorescence in buffer due to fast vibrational relaxation of the singlet excited state through internal bond rotations (Haidekker and Theodorakis 2007; Yu et al. 2015). When the fluorescent probe binds to the protein, a large fluorescence increase can be noticed due to restricted bond rotation of the fluorophore. The increase in fluorescence intensity allows measurements of interaction between the probes and the proteins. Therefore, we titrated the *Ldis*PBP1 and *Ldis*PBP2 with 6-FAM (+)-disparlure **1a** and 6-FAM (-)-disparlure *ent*-**1a** to determine the dissociation constants (K_d) as a measure of the strength of binding. The smaller the K_d, the stronger the interaction. Fig. 4 shows the isotherms for *Ldis*PBP/fluorescent disparlure enantiomer pair, for both of which we could detect significant binding affinities. The concentration dependence of fluorescent disparlure enantiomers binding to *Ldis*PBP can be described by a hyperbolic curve, as expected for a one-site binding model (Fig. 4), for which dissociation constants (K_d) could be calculated. The novel fluorescent disparlure compounds appeared to be much stronger ligands for the *Ldis*PBP1 and *Ldis*PBP2, with dissociation constants in the nanomolar range (Fig. 4, Table.2), than the fluorescent probe NPN (which had K_d values 1.3 ± 0.3 μM for *Ldis*PBP1 and 8.6 ± 0.6 μM for *Ldis*PBP2 (Gong et al. 2010).

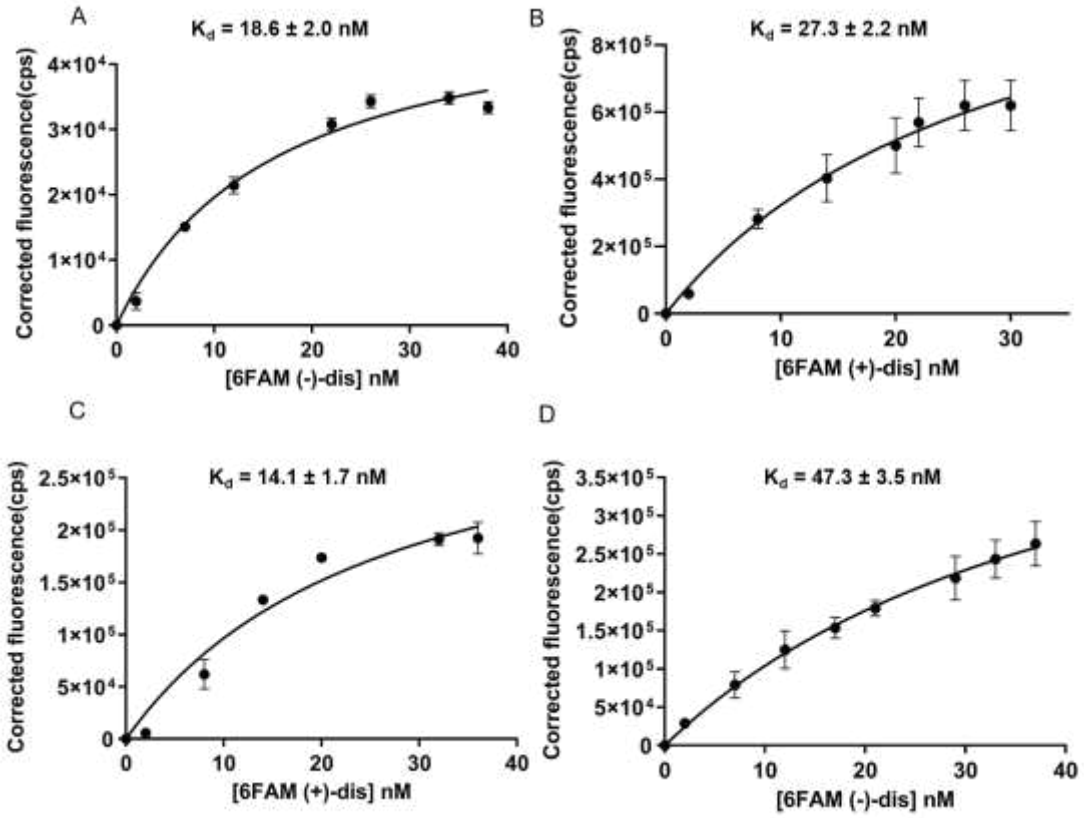

Figure4. Binding curves for 6-FAM tagged disparlure enantiomers binding with purified gypsy moth pheromone binding proteins (*Ldis*PBPs) at pH 8. **A & B** Titration of *Ldis*PBP1 with 6FAM (-)-disparlure *ent*-**1a** and (+)-disparlure **1a**, respectively. **B & C** Titration of *Ldis*PBP2 with 6FAM (+)-disparlure **1a** and (-)-disparlure *ent*-**1a**, respectively. Data represents the mean of three independent measurements. Standard errors are indicated by error bars.

Table 2. Binding of 6-FAM disparlure enantiomers **1a** and *ent*-**1a** to gypsy moth pheromone binding proteins *Ldis*PBP1 and *Ldis*PBP2.

Protein	Ligand	K_d (nM)[a]	Enantiomeric excess of the probe
*Ldis*PBP1	6-FAM (+)-disparlure 1a	27.3 ± 2.2	98.4%
	6-FAM (-)-disparlure ent-1a	18.6 ± 2.0	98.8%
*Ldis*PBP2	6-FAM (+)-disparlure 1a	14.1 ± 1.7	98.4%
	6-FAM (-)-disparlure ent-1a	47.3 ± 3.5	98.8%

[a] Values represent the mean ± S.E of 3 replicates

679 *Displacement of 6-FAM tagged disparlure by disparlure*. The fluorescence of
680 bound fluorescent probes 6-FAM (+)-disparlure **1a** and 6-FAM (-)-disparlure *ent*-**1a** was
681 followed as non-labeled disparlure (same enantiomer as the probe) was titrated, to measure
682 the binding affinities of disparlure enantiomers to *Ldis*PBP1 and *Ldis*PBP2.

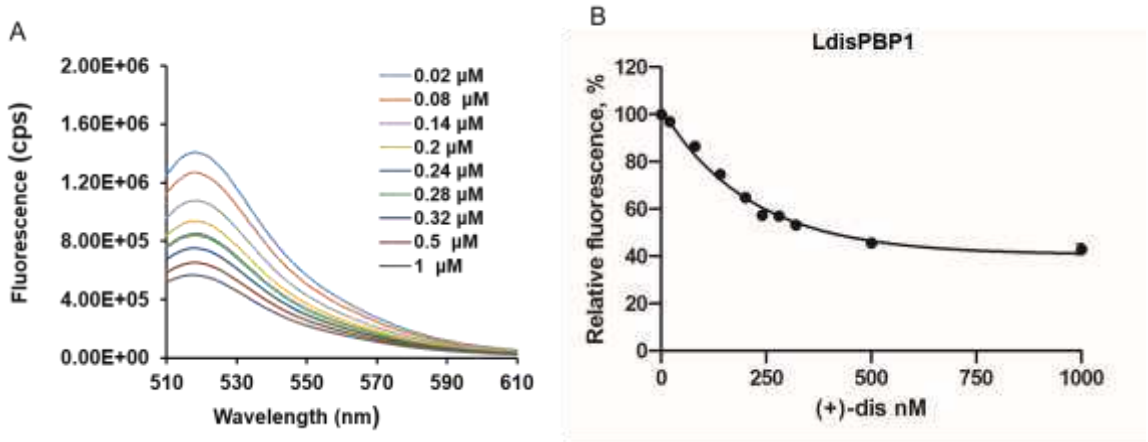

683
684

685 **Figure 5. A** Example of the decrease of 6-FAM (+)-disparlure **1a**/*Ldis*PBP1 fluorescence
686 emission intensity at maximum (520 nm) at increasing concentrations of competitor (+)-
687 disparlure (**1**). **B** Competition of 6-FAM (+)-disparlure **1a** binding to *Ldis*PBP1 (see Fig.
688 S12 (supporting information) for competition binding curves of 6-FAM (-)-disparlure *ent*-
689 **1a** with *Ldis*PBP1 and 6-FAM disparlure enantiomers with *Ldis*PBP2). Data shown are the
690 mean of 3 independent measurements. Points represent means ± S. E of 3 replicates.

691 In order to check whether fluorescent probes **1a** and *ent*-**1a** bind within the same
692 binding pocket of *Ldis*PBPs as the fluorescent probe, we titrated the equimolar mixture of
693 *Ldis*PBPs and fluorescent probes with disparlure and monitored fluorescence emission
694 spectra at 520 nm. The fluorescence emission spectra of the mixture decreased in intensity
695 upon addition of disparlure (Fig. 5A). The decrease in fluorescence emission intensity
696 suggests that the disparlure was displacing the fluorescent disparlure from binding pocket
697 of *Ldis*PBPs as it was titrated into the mixture. This decrease can be taken as a measure
698 binding affinity of disparlure for *Ldis*PBPs.

699 The displacement constant (K_i) values determined for the disparlure enantiomers in
700 competition with fluorescent probes **1a** and *ent*-**1a** binding to *Ldis*PBPs in a range between
701 132 and 211 nM. For *Ldis*PBP1, the (+)-disdparlure (**1**) and (-)-disparlure (*ent*-**1**) exhibit
702 different fluorescent probe displacement properties with K_i values of 165 and 132 nM,

703 respectively. In the case of *Ldis*PBP2, the best fluorescent probe competitor was found to
704 be (+)-disparlure (K_i = 144 nM) (Table 3). These K_i data show that the disparlure
705 enantiomers can effectively displace the corresponding enantiomer of the fluorescent probe
706 from the binding pocket. Furthermore, an estimate of the K_d values for the free disparlure
707 enantiomers from the displacement data (see derivation above) gave K_d values (Table 3)
708 within the range observed previously by other methods (*e.g*. Plettner et al. 2000). The
709 enantiomer selectivity is also consistent with previous studies.

710 **Table 3.** Inhibition of 6-FAM disparlure binding to *Ldis*PBPs by disparlure enantiomers.
711 Competitor concentrations causing a decay of fluorescence emission to half maximal
712 intensity were determined as IC_{50} values from curves resulting from competition binding
713 assays as shown in Fig. 5 and Fig. S12 (supporting information). K_i values were calculated
714 according to $K_i = [IC_{50}]/(1+[6\text{-FAM dis}]/(K_{6\text{-FAM dis}})$. [6-FAM dis] = free 6-FAM dis
715 concentration; $K_{6\text{-FAM}}$ dis = dissociation constant (K_d) for *Ldis*PBP/6-FAM dis.

Protein	Competitor	IC_{50} (nM) [a]	K_i [b]	K_d (µM) [c]
*Ldis*PBP1	(+)-disparlure	410 ± 4.6	165 ± 1.9	4.5 ± 0.4
	(-)-disparlure	414 ± 9.8	132 ± 2.3	2.5 ± 0.3
*Ldis*PBP2	(+)-disparlure	556 ± 10	144 ± 2.6	2.0 ± 0.3
	(-)-disparlure	210 ± 4.8	211 ± 4.9	10.0 ± 6.4

716 [a] Values are the ± S. E of 3 replicates. [b] Calculated from the IC_{50} and dissociation constants of the
717 ligand (see above). [c] Calculated from the K_d (6-FAM-dis) × Ki = K_d (disparlure).

718 ## Discussion

719 The results show that the 6-FAM tagged disparlure enantiomers **1a** and *ent*-**1a**
720 bound to both *Ldis*PBP1 and *Ldis*PBP2 with nanomolar dissociation constants. When
721 binding affinities of the *Ldis*PBPs for the 6-FAM tagged disparlure enantiomers were
722 compared, *Ldis*PBP1 had significantly higher affinity towards 6-FAM (-)-disparlure
723 whereas *Ldis*PBP2 bound the 6-FAM (+)-disparlure more strongly (Table 2). This is
724 consistent with the body of previous equilibrium dissociation studies on *Ldis*PBP1 and
725 *Ldis*PBP2 with (+)-disparlure (**1**) and (-)-disparlure (*ent*-**1**). *Ldis*PBP1 binds preferentially
726 to (-)-disparlure (*ent*-**1**) whereas *Ldis*PBP2 prefers (+)-disparlure (**1**) (Plettner et al. 2000;
727 Yu and Plettner 2013). Similarly, multiple studies with the NPN displacement assay have

shown that PBPs bind pheromone components selectively. For example, PBP2 and PBP3 from the Chinese silk oak moth, *Antheraea pernyi* and the giant silk moth, *Antheraea polyphemus*. preferentially binds to one pheromone component, (*e.g*. the aldehyde [(*E*,*Z*)-6,11-hexadecadienal] for PBP2), whereas PBP3 prefers the other pheromone component [(*E*,*Z*)-6,11-hexadecadienyl acetate] (Maida et al. 2003). A difference in pheromone binding affinity has been observed for PBP3 from *Ostrinia furnacalis* which binds strongly to sex pheromone components E12-14:OAc and Z11-14:OAc, but PBP4 and PBP5 bind selectively to E12-14:OAC and Z11-14:OAc, respectively (Zhang et al. 2017). Similarly, selective sex pheromone binding by PBPs has been observed for PBP1 and PBP2 of the tea geometrid moth *Ectropis obliqua* (Sun et al. 2019; Yan et al. 2020) and PBP2 of the tobacco budworm *H. virescens* (Große-Wilde et al. 2007).

Our finding of the same enantioselectivity of the two PBPs from the gypsy moth and K_d values in the same order as previously determined, shows that the probes we have prepared here can be used for more detailed studies of PBP-ligand kinetics than were possible before. This, in turn, will help us understand the mechanism by which these pheromones are bound.

Acknowledgments

This work was funded by the Natural Sciences and Engineering Research Council (NSERC) of Canada, Discovery grant (# 06088), Discovery grant accelerator supplement (# 477793) and by Simon Fraser University (stipend support to GRP). We thank Dr. Mailyn Terrado for her assistance in the production and purification of the PBPs.

Declarations

Conflict of interest: none
Availability of data: spectra are shown in the supplemental information.
Author's contributions: GRP synthesis and experimentation, writing of the manuscript; EP overseeing of the project, data review and editing of the manuscript
Ethics approval: none was required for this work; we have a biosafety permit.
Consent: both authors agree on the content and have agreed to publish this work.

References

Amatore M, Beeson TD, Brown SP, MacMillan DWC (2009) Enantioselective linchpin catalysis by SOMO catalysis: an approach to the asymmetric α-chlorination of aldehydes and terminal epoxide formation. Angew Chem Int Ed 48:5121–5124. https://doi.org/10.1002/anie.200901855

Ban L, Zhang L, Yan Y, Pelosi P (2002) Binding properties of a locust's chemosensory protein. Biochem Biophys Res Commun 293:50–54. https://doi.org/10.1016/S0006-291X(02)00185-7

Gong Y, Pace TCS, Castillo C, Bohne C, O'Neill MA, Plettner E (2009) Ligand-interaction kinetics of the pheromone-binding protein from the gypsy moth, L. dispar: insights into the mechanism of binding and release. Chem Biol 16:162–172. https://doi.org/10.1016/j.chembiol.2009.01.005

Gong Y, Tang H, Bohne C, Plettner E (2010) Binding conformation and kinetics of two pheromone-binding proteins from the gypsy moth Lymantria dispar with biological and nonbiological ligands. Biochemistry 49:793–801. https://doi.org/10.1021/bi901145a

Gong Y, Plettner E (2011) Effects of Aromatic Compounds on Antennal Responses and on the Pheromone-Binding Proteins of the Gypsy Moth (Lymantria dispar) Chem. Senses 36: 291-300. https://doi:10.1093/chemse/bjq130

Große-Wilde E, Gohl T, Bouché E, Breer H, Krieger J (2007) Candidate pheromone receptors provide the basis for the response of distinct antennal neurons to pheromonal compounds. Eur J Neurosci 25:2364–2373. https://doi.org/10.1111/j.1460-9568.2007.05512.x

Haidekker MA, Theodorakis EA (2007) Molecular rotors—fluorescent biosensors for viscosity and flow. Org Biomol Chem 5:1669–1678. https://doi.org/10.1039/B618415D

Honson N, Johnson MA, Oliver JE, Prestwich GD, Plettner E (2003) Structure–activity studies with pheromone-binding Pproteins of the gypsy moth, Lymantria dispar. Chem Senses 28:479–489. https://doi.org/10.1093/chemse/28.6.479

Kang B, Britton R (2007). A general gethod for the synthesis of nonracemic trans-epoxides: concise syntheses of trans-epoxide-containing insect sex pheromones. Org Lett 9:5083–5086. https://doi.org/10.1021/ol702273n

Krieger J, Breer H (1999) Olfactory reception in invertebrates. Science 286:720–723. https://doi.org/10.1126/science.286.5440.720

Maida, R., Ziegelberger, G., Kaissling, K.-E., 2003. Ligand binding to six recombinant pheromone-binding proteins of Antheraea polyphemus and Antheraea pernyi. J. Comp. Physiol. B 173, 565–573. https://doi.org/10.1007/s00360-003-0366-4

McAffee A, Chapman A, Iovinella I, Gallagher-Kurtzke Y, Collins TF, Higo H, Madilao LL, Pelosi P, Foster LJ (2018) A death pheromone, oleic acid, triggers hygienic behavior in honey bees (Apis mellifera L.) Nature Scientific Reports 8:5719 DOI:10.1038/s41598-018-24054-2

Pinnelli GR, Terrado M, Hillier NK, Lance DR, Plettner E (2019) Synthesis of isotopically labelled disparlure enantiomers and application to the study of enantiomer discrimination in gypsy moth pheromone-binding proteins. Eur J Org Chem 2019:6807–6821. https://doi.org/10.1002/ejoc.201901164

Plettner E, Lazar J, Prestwich EG, Prestwich GD (2000) Discrimination of pheromone enantiomers by two pheromone binding proteins from the gypsy moth Lymantria dispar. Biochemistry 39:8953–8962. https://doi.org/10.1021/bi000461x

Sandler BH, Nikonova L, Leal WS, Clardy J (2000) Sexual attraction in the silkworm moth: structure of the pheromone-binding-protein–bombykol complex. Chem Biol 7:143–151. https://doi.org/10.1016/S1074-5521(00)00078-8

Sanes JT, Plettner E (2016) Gypsy moth pheromone-binding protein-ligand interactions: pH profiles and simulations as tools for detecting polar interactions. Arch Biochem Biophys 606:53–63. https://doi.org/10.1016/j.abb.2016.07.008

Sato K, Pellegrino M, Nakagawa T, Nakagawa T, Vosshall LB, Touhara,K (2008) Insect olfactory receptors are heteromeric ligand-gated ion channels. Nature 452:1002–1006. https://doi.org/10.1038/nature06850

Shibuya GM, Kanady JS, Vanderwal CD (2008) Stereoselective dichlorination of allylic alcohol derivatives to access key stereochemical arrays of the chlorosulfolipids. J Am Chem Soc 130:12514–12518. https://doi.org/10.1021/ja804167v

Sjöback R, Nygren J, Kubista M (1995) Absorption and fluorescence properties of fluorescein. Spectrochim. Acta A Mol Biomol Spectrosc 51:L7–L21. https://doi.org/10.1016/0584-8539(95)01421-P

Sun L, Wang Q, Zhang Y, Tu X, Yan Y, Wang Qi, Dong K, Zhang Yo, Xiao Q (2019) The sensilla trichodea-biased EoblPBP1 binds sex pheromones and green leaf volatiles in Ectropis obliqua Prout, a geometrid moth pest that uses Type-II sex pheromones. J Insect Physiol 116:17–24. https://doi.org/10.1016/j.jinsphys.2019.04.005

Terrado M, Okon M, McIntosh LP, Plettner E (2020) Ligand- and pH-Induced structural transition of gypsy moth Lymantria dispar pheromone-binding protein 1 (LdisPBP1). Biochemistry 59:3411–3426. https://doi.org/10.1021/acs.biochem.0c00592

Vogt RG, Kohne AC, Dubnau JT, Prestwich GD (1989) Expression of pheromone binding proteins during antennal development in the gypsy moth Lymantria dispar. J Neurosci. 9:3332–3346. https://doi.org/10.1523/JNEUROSCI.09-09-03332.1989

Wicher D, Schäfer R, Bauernfeind R, Stensmyr MC, Heller R, Heinemann SH, Hansson BS (2008) Drosophila odorant receptors are both ligand-gated and cyclic-nucleotide-activated cation channels. Nature 452:1007–1011. https://doi.org/10.1038/nature06861

Yan Y, Zhang Yu, Tu X, Wang Q, Li Y, Li H, Wang Qi, Zhang Yo, Sun L (2020) Functional characterization of a binding protein for Type-II sex pheromones in the tea geometrid moth Ectropis obliqua Prout. Pestic Biochem Physiol 165:104542. https://doi.org/10.1016/j.pestbp.2020.02.008

Yu WT, Wu TW, Huang CL, Chen IC, Tan KT (2015) Protein sensing in living cells by molecular rotor-based fluorescence-switchable chemical probes. Chem Sci 7:301–307. https://doi.org/10.1039/C5SC02808F

Yu Y, Plettner E (2013) Enantiomer and conformer recognition of (+) and (-)-disparlure and their analogs by the pheromone binding proteins of the gypsy moth, Lymantria dispar. Bioorg Med. Chem 22:1811-1822. https://doi.org/10.1016/j.bmc.2013.01.043

Zhang T, Sun Y, Wanner KW, Coates BS, He K, Wang Z (2017) Binding affinity of five PBPs to Ostrinia sex pheromones. BMC Mol Biol 18:4. https://doi.org/10.1186/s12867-017-0079-y

Zhang XF, Zhang J, Liu L (2014) Fluorescence properties of twenty fluorescein derivatives: lifetime, quantum yield, absorption and emission spectra. J Fluoresc 24:819–826. https://doi.org/10.1007/s10895-014-1356-5

Supplementary Files

This is a list of supplementary files associated with this preprint. Click to download.

- SupportinginformationJ.Chem.Ecol2021GPJune26.docx